OFFICE OF NAVAL RESEARCH
DEPARTMENT OF THE NAVY
CONTRACT N00014-67-A-00094-0007

FINAL REPORT

WALL EFFECTS IN CAVITY FLOWS

BY

T. YAO-TSU WU
ARTHUR K. WHITNEY
J. D. LIN

DIVISION OF ENGINEERING AND APPLIED SCIENCE
CALIFORNIA INSTITUTE OF TECHNOLOGY
PASADENA, CALIFORNIA

REPORT NO. E-111A.5

AUGUST 1969

Division of Engineering and Applied Science
California Institute of Technology
Pasadena, California

FINAL REPORT

WALL EFFECTS IN CAVITY FLOWS

Contract N00014-67-A-0094-0007

T. Yao-tsu Wu

Arthur K. Whitney

J. D. Lin

This research was carried out under the Naval Ship Systems Command General Hydromechanics Research Program SR 009 01 01, and Hydrofoil Advanced Development Program S46-06, administered by the Naval Ship Research and Development Center. Prepared under Contract N00014-67-A-0094-0007

Report No. E111A.5 August 1969

FOREWORD

The research program under Contract N00014-67-A-0094-0007 was given to commence on 1 February 1966, and has been completed on 31 January 1969. This report concludes the work carried out under this Contract. The objective of the present report is to indicate the scope of work performed, to state the progress and contributions achieved, and to report the recent results obtained under this program.

ABSTRACT

The wall effects in cavity flows past an arbitrary two-dimensional body is investigated for both pure-drag and lifting cases based on an inviscid nonlinear flow theory. The over-all features of various theoretical flow models for inviscid cavity flows under the wall effects are discussed from the general momentum consideration in comparison with typical viscous, incompressible wake flows in a channel. In the case of pure drag cavity flows, three theoretical models in common use, namely, the open-wake, Riabouchinsky and re-entrant jet models, are applied to evaluate the solution. Methods of numerical computation are discussed for bodies of arbitrary shape, and are carried out in detail for wedges of all angles. The final numerical results are compared between the different flow models, and the differences pointed out. Further analysis of the results has led to development of several useful formulas for correcting the wall effect. In the lifting flow case, the wall effect on the pressure and hydrodynamic forces acting on arbitrary body is formulated for the choked cavity flow in a closed water tunnel of arbitrary shape, and computed for the flat plate with a finite cavity in a straight tunnel.

WALL EFFECTS IN CAVITY FLOWS

1. Introduction

In correlating the experimental results of water-tunnel tests on cavity flows with the corresponding unbounded flow case, it is necessary to know the effects due to the presence of tunnel flow boundaries. The wall effects in cavity flows have been generally recognized to be considerably more important and more difficult to determine than those in the wind-tunnel or water-tunnel tests of non-separated, single-phase flows past a body. A primary reason for this is that the presence of a cavity boundary renders the problem nonlinear, consequently the configuration of the body-cavity system will change as the wall spacing or the cavitation number varies, whereas in non-separated or non-cavitating flows the body shape always remains the same. Partly due to this difficulty, not an accurate formula or rule for the wall correction has been established, at least not in the general case of a finite cavity attached to a body of arbitrary bluntness. A principal objective of this study is to investigate thoroughly the relevant flow parameters in order to establish a simple wall correction rule.

The physical flow boundaries in the test section of water tunnels may be classified in three different types: (a) rigid walls of closed tunnels, (b) a free surface of constant pressure if the tunnel uses a free jet, and (c) a combination of free and solid surfaces such as in a bounded jet tunnel or in a free surface channel with a rigid bottom and sides. Presence of these flow boundaries will introduce several significant effects: (i) First, in dealing with the potential portion of the flow, these flow boundaries will impose a condition either on the flow direction at rigid walls or on the pressure at a free surface. (ii) In the case of closed tunnels, the boundary layer built up at the solid wall surface will generate a longitudinal pressure gradiant in the working section, and may even produce, depending on the configuration of the model installation and the tunnel cross-section, a secondary flow which may further change the pressure field. Moreover, the lateral constraint due to the tunnel walls will result in a higher velocity outside the boundary layer and hence a greater skin friction at the wetted body surface. In general practice, however, the characteristic Reynolds number Re is sufficiently high such that the boundary-layer-induced pressure field is of order $O(Re^{-\frac{1}{2}})$ (or at most of order $O(Re^{-\frac{1}{2}} \log Re)$ for lifting flow experiments) and is hence of secondary importance. (iii) In case the cavity boundary detachment from a curved body is smooth (i.e., with a finite curvature, such as from a circular cylinder), the point of detachment on the body will depend on both the cavitation number and the wall spacing. In such cases, correlation between tunnel experiments and the unbounded flow theory would be even more complicated. In the present work, efforts will be aimed at investigating effect (i) for both the pure drag and the lifting flows so that this primary effect can be clarified first. Effect (ii) can be evaluated with some modifications of the present formulation by taking the boundary layer into account. In practice, this viscous effect arising in the presence of tunnel walls can be effectively compensated for at one Reynolds number by having slightly diverging walls, or with adjustable walls. Effect (iii) is however beyond the scope of the present study.

Several problems of wall effects have been discussed previously for some special cases. The choked cavity flow case (i.e., when the cavity is infinitely long in a channel or in a free jet) has attracted early attention due to its relative simplicity. This problem has been treated for symmetric wedges by Birkhoff, Plesset and Simmons (1950). For a symmetric body of cross-sectional area A, placed symmetrically in the tunnel, experiencing a drag D in a choked cavity flow which has upstream velocity U and pressure p_∞, let two drag coefficients be defined as

$$C_D = D/\left(\tfrac{1}{2}\rho U^2 A\right) \qquad C_D' = D\Big/\left(\tfrac{1}{2}\rho q_c{}^2 A\right) \tag{1}$$

where q_c is the constant velocity at the cavity boundary. In the case of a flat plate set broadwise to the flow, the theoretical results of Birkhoff, Plesset and Simmons show that the conventional drag coefficient C_D is almost insensitive to the width of the free jet (down to the body width) but depends strongly on the spacing of the channel walls, whereas C_D' is found to be insensitive to either the channel spacing or the width of the free jet. (Of course, for a plate in a free jet the two velocities U and q_c are equal.) These results had been predicted earlier by Valcovici (1913) based on methods suggested by Prandtl. Now, by Bernoulli's theorem,

$$p + \tfrac{1}{2}\rho q^2 = p_\infty + \tfrac{1}{2}\rho U^2 = p_c + \tfrac{1}{2}\rho q_c^2 = p_b + \tfrac{1}{2}\rho V^2 = p_s \tag{2}$$

where p_c is the cavity pressure, p_s the stagnation pressure, and p_b is another reference pressure associated with a third reference velocity V, C_D and C_D' are seen to be related by

$$C_D = (q_c/U)^2 C_D' = (1+\sigma)C_D' \tag{3}$$

where σ is the conventional cavitation number,

$$\sigma = (p_\infty - p_c)\Big/\left(\tfrac{1}{2}\rho U^2\right) = (q_c/U)^2 - 1 \quad . \tag{4}$$

In view that C_D' is nearly constant (which is 0.88 for the flat plate) and the factor $(1+\sigma)$ gives an accurate dependence of C_D on σ for a flat plate in an unbounded flow (for $0 < \sigma < 1$, see, e.g., Gilbarg (1961), Wu (1968)), this result has led Birkhoff (1950) to assert the stronger "principle of stability of the pressure coefficient": that for an obstacle of given shape in a water tunnel (or jet) the pressure coefficient

$$C_p' \equiv \frac{p-p_c}{\frac{1}{2}\rho q_c^2} = 1 - \left(\frac{q}{q_c}\right)^2 , \quad \text{instead of} \quad C_p \equiv \frac{p-p_\infty}{\frac{1}{2}\rho U^2} = 1 - \left(\frac{q}{U}\right)^2 , \tag{5}$$

is insensitive to the presence of walls and changes in the cavitation number σ. This principle, elegant and useful it may be for blunt bodies, unfortunately does not possess a general validity. In fact, as the result of this work will show later, the wall effects on both C_D and C_D', at fixed cavitation number σ above its choked flow value, are rather insignificant for blunt bodies. For symmetric wedges, the wall effect on C_D increases with decreasing wedge angle and this effect on C_D' is actually more pronounced than on C_D. Furthermore, even in the unbounded flow case, the nonlinear deviation of $C_D(\sigma)$ from the factor $(1+\sigma)$ becomes greater, the thinner the body becomes, or the smaller is the incidence angle of a lifting surface (see Wu (1956), Wu and Wang (1964a)). This feature of the dependence of C_D on σ weakens further the argument underlying the principle mentioned above. Another exceptional case is that when a flat plate is situated outside of the mouth of a bounded jet, this principle is appreciably violated, as shown by the numerical results of Birkhoff, Plesset, Simmons (1950).

For the more general case of a finite cavity formation behind a given body placed symmetrically in a bounded stream, various attempts have been made with resort to different theoretical flow models. The Riabouchinsky model has been adopted by Cisotti (1922) for cavity flow past a plate in a channel, by Caywood (1946) for wedges, by Birkhoff, Plesset and Simmons (1952) for a plate either in a channel or in a free jet. The re-entrant jet model has been used by Gurevich (1953) for a wedge in a channel. The open wake model of Joukowsky and Roshko, which turns out to be the simplest in numerical details, has not been employed before (insofar as the authors are aware of). This is taken up here with the other models in formulating the general problem of an arbitrary body placed in a channel.

An entirely different approach to this problem for thin bodies at small incidences is based on the linearized cavity flow theory. This linearized theory has been developed for wall effect problems by Cohen and Di Prima (1958), Cohen and Gilbert (1957), Cohen, Sutherland and Tu (1957), and by Fabula (1964). Some comparison between the nonlinear and linear theories will be made in this study.

The problem of wall effects on lifting cavity flows is more complicated due to the lack of a basic symmetry. The case of choked flow past an inclined flat plate within a straight channel has been investigated by Ai (1965). A linearized theory for choked flows past vented or cavitating hydrofoils has been developed by Fabula (1964). Ai's theory is generalized here to account for a body of arbitrary shape. A general formulation is presented here to treat the finite cavity flow based on the open wake model.

Recently, Brennen (1969) evaluated the wall effect for axi-symmetric flows with a finite cavity past a disk and a sphere; he also obtained some new experimental results. In his theory the Riabouchinsky model is adopted to represent the finite cavity. One important aspect of Brennen's relaxation method is that the flow is bounded laterally by a concentric cylinder of various sizes, down to the smallest that produces the choked flow at a given cavitation number, and the unbounded flow case is reached by extrapolation. The numerical results therefore furnish useful information about the wall effect in three-dimensions.

Experimental studies designed to investigate primarily the wall effects in cavity flows have received increasing attention recently. A review of these activities has been given by Morgan (1966). Dobay (1967) investigated experimentally the blockage effects on cavity flows past a circular disc, set normal to the flow, of three different sizes. These extensive experiments showed that choking occurred even with these relatively small discs (disc diameter-to-tunnel down to 1/36). Similar findings have been reported by Barr (1966). A recent survey and discussion of this subject has also been given by Waid (1968).

A clear understanding of the wall effects in wake or cavity flows is necessary to interpret correctly the experimental result. Grove et al (1964) investigated experimentally the steady separated flow past a circular cylinder (of diameter d) in an oil tunnel (of spacing h) with the Reynolds number R up to about 300. For the case $d/h = 0.05$, the rear pressure coefficient was found to reach the asymptote -0.45 for $R > 25$ (up to $R = 177$). It is further conjectured that the pressure profile for $d/h = 0.05$ has already reached the limiting form as $d/h \to 0$ (the unbounded flow case). This final extrapolation seems misleading since a simple estimate (e.g. by using Eq. (10) below) indicates that the flow state at hand is right in the neighborhood of the choked flow state.

Finally, it may be mentioned here that a series of experiments has been carried out by Meijer (1967) in an investigation (collaborated with one of the present authors, TYW) of the tunnel wall effect and the viscous effect at a sharp corner of the body. An empirical method for correcting the wall effect was chosen, which is based on a different pressure coefficient C_p'' and cavitation number σ'', defined as

$$C_p'' = \frac{p-p_b}{\frac{1}{2}\rho V^2} = 1 - \frac{q}{V}^2 \quad , \quad \sigma'' = \frac{p_b-p_c}{\frac{1}{2}\rho V^2} \quad , \quad C_D'' = \frac{D}{\frac{1}{2}\rho V^2 A} \quad , \tag{6}$$

where p_b is the minimum pressure and V is the corresponding maximum velocity on the tunnel wall (measured at a point on the tunnel wall opposite to the maximum cross-section of the cavity, see the point B in Fig. 3 of the Riabouchinsky model). This $C_p''(\sigma'')$ has been found to correlate very satisfactorily with the theoretical values of $C_p(\sigma)$ for an unbounded flow, as supported by a number of tests with models of three different sizes. Some theoretical justification is being sought in this study.

2. Theoretical Models for Inviscid Cavity Flows; Momentum Considerations

It has been known that the theoretical models in common use for treating steady inviscid cavity flows can predict hydrodynamic forces acting on blunt obstacles with differences so small that they are usually beyond the limit of experimental accuracy (see, e.g., Gilbarg (1961)). It is also known that these models, when applied to unsteady cavity flow problems, have yielded appreciably different results (see Wang and Wu (1963)). Since the viscous effects of the real fluid in the wake are approximated by different artifices in different models, and the cavity drag is distributed at different rates in different regions, it should be of value to examine these models in the presence of strong wall effects. This will be done in two parts. First, the over-all features will be studied in the light of simple momentum consideration. The rest will be left with the detailed analysis. The final results exhibit significant differences between the three models tried out, when applied to thin obstacles. This finding therefore sets the stage for further experimental investigations for a crucial appraisal of the theoretical models.

Before we deal with the inviscid cavity flow or wake flow models, let us consider a typical viscous, incompressible flow produced in an infinitely long straight channel by a blunt body which is propelled along the channel axis by an external force, moving at sufficiently high Reynolds number Re such that a recirculating near wake (or a finite cavity in a two-phase flow) is established. For simplicity, the additional viscous effect due to the boundary layer built up along the channel walls will be singled out by assuming that the walls can be made to move with an appropriate tangential velocity so as to eliminate the boundary layer altogether. Then, with respect to the body frame, the upstream velocity will be denoted by U, and the pressure by p_∞ (see Fig.1a). At large distances downstream (say for $x \gg \rho U^2 S^{3/2}/D$, where S is the cross-sectional area of the channel and D is the drag of the body), so that after the turbulent far wake has spread uniformly across the channel, or even after the turbulence is dissipated and degenerated into a laminar flow, the mean velocity will again be uniform, equal to U on account of the continuity, but the pressure, after full recovery of the kinetic energy, will be p_b say, which must be less than p_∞, since by the simple momentum consideration

$$D = (p_\infty - p_b)D \quad , \quad \text{or} \quad C_p^- = \frac{p_\infty - p_b}{\frac{1}{2}\rho U^2} = \frac{A}{S} C_D \quad , \tag{7}$$

A being the body section area and C_D being defined by (1). Thus the wall effect here is to reduce the momentum defect to zero, and to give rise to an under-pressure in the downstream. This underpressure coefficient C_p^- diminishes in proportion to the ratio A/S, as $A/S \to 0$, since C_D must remain finite. (In plane flows, S is replaced by the channel spacing h, and A by the body width ℓ.)

We now turn to consider the cavity flow models for an arbitrary body placed in a straight channel, with a finite cavity formation. Although they have been applied exclusively to plane flow analysis, the following momentum theorems hold also valid for the three-dimensional case so long as the flow is symmetric about a $z = 0$ plane.

2.1 Open wake model

According to this model, which is due to Joukowsky (1890), Roshko (1954), and Eppler (1954) and modified by Wu (1962), the dividing streamline starts with a uniform velocity U and pressure p_∞ at upstream infinity, flows tangentially to the body surface (ED and ED' in the cross-sectional view of Fig. 1b), detaches from the body at D and D' to form a cavity boundary DC and D'C' over which the flow speed assumes a prescribed constant value q_c, and the pressure p_c, then proceeds downstream along CB and C'B', approaching asymptotically parallel to the walls so that the flow cross section becomes k ($= k_1 + k_2$ in Fig. 1b), velocity becomes V, and pressure p_b. The shape of CB and C'B' is so determined that there will be no net contribution from this variable pressure part of the boundary to the force on the body. Both V and k are unknown a priori, but must satisfy the continuity equation

$$Uh = Vk \quad . \tag{8}$$

Application of the longitudinal component of the momentum theorem to the flow region gives

$$D = (p_\infty - p_c)h - (p_b - p_c)k + \rho U^2 h - \rho V^2 k$$

which becomes, upon using Bernoulli's equation (2) and continuity condition (8),

$$C_D \equiv \frac{D}{\frac{1}{2}\rho U^2 \ell} = \frac{h}{\ell}\left(\frac{V}{U} - 1\right)\left(\frac{q_c^2}{UV} - 1\right) \tag{9}$$

where ℓ denotes the lateral body width for plane flows or the body cross sectional area in three-dimensional flows.

It is of particular significance to consider the limiting case when the cavity becomes infinitely long (the so-called choked flow) as V

increases towards q_c. Let the corresponding limit of U, C_D and the cavitation number σ, with h/ℓ and q_c held fixed, be denoted by U_*, C_{D*} and σ_* respectively, then

$$C_{D_*} = \frac{h}{\ell}\left(\frac{q_c}{U_*} - 1\right)^2 = \frac{h}{\ell}\left[\sqrt{1+\sigma_*} - 1\right]^2 \quad , \tag{10}$$

σ_* is called the choking cavitation number, or the blockage constant. From (10) it follows that

$$\sigma_* = 2\left(\frac{\ell}{h}\; C_{D_*}\right)^{\frac{1}{2}} + \left(\frac{\ell}{h}\; C_{D_*}\right) > 2\left(\frac{\ell}{h}\; C_{D_*}\right)^{\frac{1}{2}} \quad . \tag{11}$$

It is to be noted that σ_* provides a lower limit of σ below which the flow is physically infeasible, and that the right hand side quantity in (11) is a quite accurate estimate of σ_* for large h/ℓ. Thus, to achieve $\sigma = 0.1$, we must have $h/\ell > 400$ if $C_{D_*} \simeq 1$.

Another point of interest is that the choking drag coefficient can be expressed in terms of the geometry by using (8). Since $U_* h = q_c k$, (10) and (3) become

$$C_{D_*} = \frac{h}{\ell}\left(\frac{h}{k} - 1\right)^2 \quad , \quad C'_{D_*} = \left(\frac{q_c}{U_*}\right)^{-2} C_{D_*} = \frac{h}{\ell}\left(1 - \frac{k}{h}\right)^2 . \tag{12}$$

In the case of bluff bodies C'_{D_*} is insensitive to ℓ/h, then

$$\frac{k}{h} = 1 - \left(\frac{\ell}{h}\; C'_{D_*}\right)^{\frac{1}{2}} \tag{13}$$

gives an estimate of k/h versus ℓ/h.

When the cavity is finite in length, we must have $U < V < q_c$. For sufficiently large h/ℓ so that $V \sim U$ (see Eq. (9)), the under-pressure coefficient at the downstream end becomes

$$C_p^- = (p_\infty - p_b)/\left(\frac{1}{2}\rho U^2\right) = (V/U)^2 - 1 \simeq \left(\frac{\ell}{h}\right)\left(\frac{2C_D}{\sigma}\right) \qquad (\sigma > \sigma_*) \quad , \tag{14}$$

thus C_p^- is proportional to ℓ/h, in agreement with (7) which is based on the viscous flow argument. However, when the cavity is also long, then by (11),

$$C_p^- \sim \left(\frac{\ell}{h} C_{D_*}\right)^{\frac{1}{2}} \qquad (\sigma = \sigma_*) \tag{15}$$

which decreases much slower with decreasing ℓ/h at the choked flow state.

2.2 Re-entrant jet model

Description of the main features of this model, which has been attributed independently to Kreisel, Gilbarg and Efros, can be found in the book article of Gilbarg (1960). As shown in Fig. 1c, let the downstream uniform state be characterized by velocity V and pressure p_b, and let the jet flow upstream through the cavity into a second Riemann sheet, terminating with the cavity surface velocity q_c across a constant section of area ℓ_j, inclined at an angle γ with the upstream flow direction. Then the continuity condition requires

$$(U - V)h = q_c \ell_j \quad . \tag{16}$$

In contrast to the open-wake model, we now have $V < U$ and hence $p_b > p_\infty$ (an over-pressure at the downstream!) as the momentum defect is partly carried off by the jet. Since the longitudinal momentum flux in the jet is $(-\rho q_c \cos\gamma)(q_c \ell_j)$, we now have the momentum equation

$$D = (p_\infty - p_c)h - (p_b - p_c)h + \rho(U^2 - V^2)h + \rho\ell_j q_c^2 \cos\gamma$$

which is reduced upon using (16) and (2) to

$$C_D = \frac{D}{\frac{1}{2}\rho U^2 \ell} = \frac{h}{\ell}\left(1 - \frac{V}{U}\right)\left(1 + \frac{V}{U} + 2\frac{q_c}{U}\cos\gamma\right) \quad . \tag{17}$$

The choked flow state cannot be readily derived from the above formulas (it can however be deduced from the analysis later), but this limit must evidently be the same as (10) and (11) in virtue of the momentum consideration, if applied directly to this state. Before the flow is choked, the over pressure at the downstream end is

$$C_p^+ = \frac{p_b - p_\infty}{\frac{1}{2}\rho U^2} = 1 - \left(\frac{V}{U}\right)^2 \simeq \left(\frac{\ell}{h}\right) C_D \Big/ \left(1 + \frac{q_c}{U}\cos\gamma\right) \quad . \tag{18}$$

2.3 Riabouchinsky model

The main features of this model are shown in the typical case of Fig. 3. Since there is no more than one distinct uniform flow state, the simple momentum argument cannot be effected to determine the drag, albeit the choked flow state must also agree with the other models. On the other hand, this model has an advantage of providing readily a point (point B in Fig. 5) at which the velocity is maximum, and pressure minimum over the entire tunnel wall. This velocity is to be used in calculating C_p'' as defined by (6).

I. Pure Drag Cavity Flows

In this part we consider the pure drag cavity flow past a symmetric body of an arbitrary shape, placed symmetrically in a straight channel of width h, with a finite cavity attached to the body, the flow being assumed to be symmetric about the central plane of the channel. The characteristic Reynolds number and the Froude number based on the body dimension are both assumed to be so large that the viscous and gravitational effects may be neglected. The solution will be determined by using three different flow models.

3. Open Wake Model

This semi-infinite open wake model has already been described in the previous section. As shown in Fig. 2, the boundaries CB and C'B' of the variable pressure part of the open wake now become straight and parallel to the x-axis by virtue of the flow symmetry. The flow region in the strip $|\psi| \leq \psi_1 = Uh/2$ of the complex potential plane $f = \varphi + i\psi$, φ being the velocity potential and ψ the stream function, is mapped into the upper half of the parametric plane $\zeta = \xi + i\eta$ by

$$\frac{df}{d\zeta} = \frac{A\zeta}{(\zeta^2+a^2)(\zeta^2+b^2)} \quad , \qquad A = \frac{1}{\pi}\, Uh(b^2-a^2) \quad , \tag{19}$$

in which the coefficient A is determined by the jump of ψ across the flow about the upstream or downstream infinity (point A or B). The corresponding regions in the z, f, and ζ-planes are shown in Fig. 2.

By denoting the x, y-velocity components by u, v, and the complex velocity by

$$w = u - iv = \frac{df}{dz} = q e^{-i\theta} \quad , \quad q = |w| \quad , \quad \theta = \tan^{-1}(v/u) \quad , \tag{20}$$

physical problems can be stated by prescribing θ at the body surface, $\theta = \beta(s)$ say, s being the arc length measured from E along ED, and by prescribing $q = q_c$ along the cavity boundary DC and D'C'. For brevity, q_c will be normalized henceforth to unity. In terms of the logarithmic hodograph variable

$$\omega = \tau + i\theta = \log \frac{1}{w} \quad , \quad \tau = \log \frac{1}{q} \quad , \tag{21}$$

the problem becomes the following Riemann-Hilbert boundary value problem:

$$\begin{aligned} &\theta(\xi, 0+) \equiv \theta^{+}(\xi) = \beta(s(\xi)) && (|\xi| < 1) \quad , \\ &\tau(\xi, 0+) = 0 && (|\xi| > 1) \quad , \\ &\omega = 0(1/\zeta) \quad \text{as} \quad |\zeta| \to \infty \quad , \end{aligned} \tag{22}$$

in which we specify $s(-\xi) = -s(\xi)$, and $\beta(-s) = -\beta(s)$. We shall also designate $\beta(\xi) \equiv \beta(s(\xi))$, with $\beta(-\xi) = -\beta(\xi)$. The solution of this problem is

$$\omega(\zeta) = \frac{1}{i\pi} \; (\zeta^2 - 1)^{\frac{1}{2}} \int_{-1}^{1} \frac{\beta(\xi) d\xi}{(\xi - \zeta)(1 - \xi^2)^{\frac{1}{2}}} \qquad (\text{Im}\zeta > 0) \tag{23}$$

in which the function $(\zeta^2 - 1)^{\frac{1}{2}}$ is analytic in the ζ-plane cut along the ξ-axis from -1 to 1, and tends to ζ as $|\zeta| \to \infty$. It is noted that the last condition in (22) is also satisfied since the integral in (23) is of order $0(\zeta^{-2})$ as $|\zeta| \to \infty$ by virtue of $\beta(\xi)$ being odd in ξ. Finally, the boundary conditions of w at the upstream and downstream infinity require

$$\log \frac{1}{U} = \omega(ia) = \frac{2}{\pi}(1+a^2)^{\frac{1}{2}} \int_0^1 \frac{\beta(\xi)\xi\, d\xi}{(\xi^2+a^2)(1-\xi^2)^{\frac{1}{2}}} , \tag{24}$$

$$\log \frac{1}{V} = \omega(ib) = \frac{2}{\pi}(1+b^2)^{\frac{1}{2}} \int_0^1 \frac{\beta(\xi)\xi\, d\xi}{(\xi^2+b^2)(1-\xi^2)^{\frac{1}{2}}} . \tag{25}$$

Equations (19) and (23) provide a parametric solution $f = f(\zeta)$, $\omega = \omega(\zeta)$. The physical plane is given by quadrature,

$$z(\zeta) = \int_0^\zeta \frac{1}{w} \frac{df}{d\zeta}\, d\zeta = \int_0^\zeta e^{\omega(\zeta)} \frac{df}{d\zeta}\, d\zeta . \tag{26}$$

Let the base chord DD' be of length ℓ, then $\ell = \mathrm{Im}(z(1) - z(-1))$, or

$$\ell = \mathrm{Im} \int_{-1}^1 e^{\omega(\zeta)} \frac{df}{d\zeta}\, d\zeta , \tag{27a}$$

and hence, after substituting (19) in (27a),

$$\lambda \equiv \frac{\ell}{h} = \mathrm{Im}\, \frac{U}{\pi} \int_{-1}^1 e^{\omega(\zeta)} \left[\frac{1}{\zeta^2+a^2} - \frac{1}{\zeta^2+b^2}\right] \zeta\, d\zeta . \tag{27b}$$

Now on the body surface, as $\eta \to 0+$,

$$\omega(\xi+i0) = \Gamma(\xi) + i\beta(\xi) , \quad \Gamma(\xi) = \frac{1}{\pi} \oint_{-1}^1 \left(\frac{1-\xi^2}{1-t^2}\right)^{\frac{1}{2}} \frac{\beta(t)dt}{t-\xi} , \tag{28}$$

where C over the integral sign indicates the Cauchy principal value. Hence the arc length s, measured from E along ED, is

$$s(\xi) = \int_0^\xi e^{\Gamma(\xi)} \frac{df}{d\xi}\, d\xi \qquad (0 \leqslant \xi \leqslant 1) . \tag{29}$$

The drag coefficient is given by (9), or after setting $q_c = 1$,

$$C_D \equiv \frac{D}{\frac{1}{2}\rho U^2 \ell} = \frac{h}{\ell}\left(\frac{V}{U} - 1\right)\left(\frac{1}{UV} - 1\right) . \tag{30}$$

The above solution may be regarded either as a direct (physical) or an inverse problem. The direct problem is prescribed by the quantities

$$P[\beta(s), \sigma, \lambda] \tag{31}$$

in which $\beta(s)$ is a known function of the arc length s, σ is taken to be greater than the blockage constant σ_* for fixed $\lambda(= \ell/h) < 1$. The inverse problem is specified by

$$P'[\beta(\xi), a, b] \qquad (-1 < \xi < 1) \tag{32}$$

in which $\beta(\xi)$ is a given function of ξ and $0 < a < b$. The inverse problem is seen to be fully determined, since if the quantities P' are prescribed, then (24), (25) provide U and V, (23) determines $\omega(\zeta)$, (27) fixes ℓ/h, z is given by (26), and finally the C_D follows from (30). On the other hand, in the direct problem with fixed detachment (from a sharp corner of the obstacle), $s(\xi)$ and $\beta(\xi) = \beta(s(\xi))$ are not known á priori. Consequently its solution involves a nonlinear integral equation (29) for $s(\xi)$ together with two parameters a, b, which must be evaluated under two functional conditions (24) and (27) for fixed U and ℓ/h. (Note that $U = (1+\sigma)^{-\frac{1}{2}}$). In the case of smooth detachment (when the body curvature is finite on both sides of the detachment point, such as detachment from a circular cylinder), an additional condition is required. The classical condition is that of Villat (1914), which can be written as $(\zeta^2 - 1)^{\frac{1}{2}} \omega'(\zeta) \to 0$ as $\zeta \to 1$. It should be noted that V

cannot be arbitrary in problem P, instead it is fixed by (25) after a, b and $\beta(\xi)$ are solved. The numerical methods of solution for calculating the direct problem have been established and discussed for the unbounded flow case by various authors (see e.g., Birkhoff and Zarantonello (1957), Gilbarg (1960), Wu (1968)) and will not be further elaborated here. Furthermore, the approximate numerical scheme devised by Wu and Wang (1964b) has been found to be very effective. These methods can also be applied to the present problem of wall effects.

Of particular interest is the simple case of symmetric wedges since in this case β is constant and the parameters become uncoupled (U is a function of "a" only, see (24)). Consequently the solution is greatly simplified by considering a mixed type problem $P''[\beta, \sigma, b]$ so that the direct problem can be solved by simple cross plotting. We proceed to evaluate the details in the following.

3.1 Symmetric wedge

For a symmetric wedge of half vertex angle $\beta\pi$, we have

$$\beta(\xi) = \text{const.} = \beta\pi \qquad (0 < \xi < 1) \quad . \tag{33}$$

Then (23) can be readily integrated, giving

$$w(\zeta) = e^{-\omega} = e^{-i\beta\pi}\left(\frac{\zeta}{1+\sqrt{1-\zeta^2}}\right)^{2\beta} \quad . \tag{34}$$

Hence conditions (24) and (25) become

$$U = [a/(1+\sqrt{1+a^2}\,)]^{2\beta} \qquad \text{or} \qquad a^{-1} = \frac{1}{2}\left(U^{-\frac{1}{2\beta}} - U^{-\frac{1}{2\beta}}\right), \tag{35}$$

$$V = [b/(1+\sqrt{1+b^2}\,)]^{2\beta} \qquad \text{or} \qquad b^{-1} = \frac{1}{2}\left(V^{-\frac{1}{2\beta}} - V^{-\frac{1}{2\beta}}\right). \tag{36}$$

Furthermore, (27) gives the base-chord to channel-width ratio as

$$\lambda \equiv \frac{\ell}{h} = \frac{2U}{\pi}(\sin\beta\pi)(b^2 - a^2)\int_0^1 \frac{(1+\sqrt{1-\zeta^2})^{2\beta}\zeta^{1-2\beta}}{(\zeta^2+a^2)(\zeta^2+b^2)}\,d\zeta \quad . \tag{37}$$

For the direct problem $P[\beta, \sigma, \ell/h]$, first a can be computed from (35) noting that $U = (1+\sigma)^{-\frac{1}{2}}$, next b can be determined from (37), and finally V is given by (36), and C_D by (30). For arbitrary β, the integral in (37) cannot be integrated in closed form. When $\beta = m/n$, m and n being integers, appropriate changes of variables can reduce the integrand to a rational fraction, which can then be evaluated in closed form. In particular, for the flat plate, $\beta = 1/2$, the result is rather simple

$$\frac{\ell}{h} = \left(1 - \frac{U}{V}\right) + \frac{2U}{\pi}\left\{\left(\frac{1}{V} - V\right)\tan^{-1}V - \left(\frac{1}{U} - U\right)\tan^{-1}U\right\} \quad . \tag{38}$$

However, for a wide range of β, it is more convenient to evaluate the integral numerically.

In order to determine the lower limit of σ for fixed ℓ/h, we consider below the asymptotic limit of choked flow.

The choked flow state is reached as $b \to \infty$, or equivalently, as $V \to 1$. The corresponding limit of a and U, for fixed β and ℓ/h, will be denoted by a_* and U_* which are related by $U_* = U(a_*)$, $U(a)$ being given by (35). By letting $b \to \infty$ in (37), we obtain

$$\frac{\ell}{h} = \frac{2U_*}{\pi}\sin\beta\pi\int_0^1 (1+\sqrt{1-\zeta^2})^{2\beta}\zeta^{1-2\beta}\frac{d\zeta}{\zeta^2+a_*^2} \quad , \tag{39}$$

which determines $a_* = a_*(\ell/h, \beta)$. The corresponding drag coefficient at the choked condition is

$$C_{D_*} = \frac{h}{\ell}\left(\frac{1}{U_*} - 1\right)^2 = \frac{h}{\ell}\left[\sqrt{1+\sigma_*} - 1\right]^2 \quad . \tag{40}$$

In particular, we deduce from (38) for the flat plate, $\beta = \frac{1}{2}$,

$$\frac{\ell}{h} = (1-U_*) \left[1 - \frac{2}{\pi}(1+U_*)\tan^{-1} U_*\right] . \tag{41}$$

The choked flow results (39) and (40) have been computed numerically for several values of β, as shown in Fig. 3. In general, it can be seen (for example, by differentiating (39) with respect to a_* and by some appropriate partial integrations) that for $0 < \beta < 1$, ℓ/h decreases monotonically with increasing a_* (or U_*). It can also be seen (but more involved) that C_{D_*} decreases with U_* increasing (or σ_* decreasing). These salient features can be clearly seen from Fig. 3.

From this behavior of ℓ/h it also follows from (37) (for example, by partial fraction and comparison) that before the tunnel is choked, the following inequalities $a < a_*$, $U < U_*$ (and hence $\sigma > \sigma_*$) must hold. The wall effect on C_D has been computed, with $U < U_*$, for several values of β and ℓ/h, the final results will be presented in Section 6 together with the other two flow models for comparison and discussion.

The wall effect diminishes as $\ell/h \to 0$; this limit is reached as $b \to a$ (or $V \to U$). In this limit, the drag coefficient $C_D(\sigma, \beta, \ell/h)$ tends to its value in unbounded flow, $C_{D_o}(\sigma, \beta)$, which can be deduced from (30), (36) and (37) by applying l'Hospital's rule, giving

$$C_{D_o}(\sigma,\beta) = \frac{1}{U^2}\left(\frac{1}{U} - U\right) \Big/ \left(\frac{\partial\lambda}{\partial b}\right)_{b=a} \left(\frac{\partial b}{\partial V}\right)_{V=U}$$

$$= \frac{\pi\beta}{\sin\beta\pi}\left(\frac{U^{-1}-U}{U^{-1/\beta}-U^{1/\beta}}\right)\frac{2(1+\sigma)}{a^4 C_o} ,$$

$$C_o = \int_0^1 \frac{(1+\sqrt{1-\zeta^2})^{2\beta}\,\zeta^{1-2\beta}}{(\zeta^2+a^2)^2}\,d\zeta \quad . \tag{42}$$

This result has been obtained previously by Wu and Wang (1964a). The above drag coefficient $C_{D_o}(\sigma, \beta)$ for unbounded flow is shown in Fig. 4 for comparison with the results based on the Riabouchinsky and re-entrant jet models.

4. Riabouchinsky Model

We now apply the Riabouchinsky model to evaluate the pure drag cavity flow past a symmetrical body of an arbitrary shape placed in a channel. The particular case of the flat plate has been dealt with by Birkhoff, Plesset and Simmons(1952).

The corresponding regions in the z- and f-planes are shown together with the parametric ζ-plane in Fig. 5. The upper half strip in the f-plane is mapped into the upper half ζ-plane by the general Schwarz-Christoffel transformation (see Gilbarg 1949)):

$$\frac{df}{d\zeta} = \frac{A\zeta}{(\zeta^2+a^2)(\zeta^2+b^2)^{\frac{1}{2}}} \quad , \qquad A = \frac{1}{\pi} Uh(b^2-a^2)^{\frac{1}{2}} \quad , \tag{43}$$

in which the coefficient A is determined by the local behavior of f at the point $\zeta = ia$. The function $(\zeta^2+b^2)^{\frac{1}{2}}$ is analytic in the ζ-plane cut from $\zeta = -ib$ to $\zeta = ib$, and $(\zeta^2+b^2)^{\frac{1}{2}} \to \zeta$ as $|\zeta| \to \infty$. The boundary values of $\omega = \tau + i\theta$ again assume the same form as (22), though the symbol $\zeta = \xi + i\eta$ must be referred to the present problem. (Here we note that $\theta = 0$ on BC due to the flow symmetry.) It therefore follows that the parametric solution $\omega = \omega(\zeta)$, the velocity condition $\omega(ia) = -\log U$, $z = z(\zeta)$, the base chord ℓ, the arc length $s(\xi)$ can again be expressed formally by equations (23), (24), (26), (27a), and (29) respectively. The velocity V now gives the magnitude of the flow velocity at point B, which is the maximum value achieved by the velocity along the entire wall. Thus formally the numerical solution for an arbitrary body shape can be carried out by the same procedure as described in the previous case, except with $df/d\zeta$ replaced by the above equation. This completes our solution.

The drag on the body can be calculated by integrating the pressure over the body surface, giving

$$D = 2\,\mathrm{Im}\int_{Z_E}^{Z_D}(p-p_c)dz = \mathrm{Im}\,\rho\int_0^1 \frac{1-w\bar{w}}{w}\frac{df}{d\zeta}d\zeta = \mathrm{Im}\,\rho\int_0^1\left(\frac{1}{w}+w\right)\frac{df}{d\zeta}d\zeta\ . \tag{44}$$

4.1 Symmetric wedge

For a symmetric wedge of half vertex angle $\beta\pi$, $w(\zeta)$ is again given by (34), and (35) remains valid to assure $w(ia) = U$. The ratio ℓ/h, by (27a), now becomes

$$\frac{\ell}{h} = \frac{2U}{\pi}(\sin\beta\pi)(b^2-a^2)^{\frac{1}{2}}\int_0^1 \frac{(1+\sqrt{1-\zeta^2}\,)^{2\beta}\zeta^{1-2\beta}}{(\zeta^2+a^2)(\zeta^2+b^2)^{\frac{1}{2}}}d\zeta\ . \tag{45}$$

Finally, (44) gives the value of the drag coefficient

$$C_D = \frac{2\sin\beta\pi}{\pi U}\left(\frac{h}{\ell}\right)(b^2-a^2)^{\frac{1}{2}}\int_0^1 \frac{(1+\sqrt{1-\zeta^2}\,)^{2\beta}-(1-\sqrt{1-\zeta^2}\,)^{2\beta}}{(\zeta^2+a^2)(\zeta^2+b^2)^{\frac{1}{2}}}\zeta^{1-2\beta}d\zeta\ . \tag{46}$$

The numerical method of solution for arbitrary angle β is again very much the same as described in the previous case. In particular, for the flat plate, $\beta = 1/2$, the above integrals can be evaluated in terms of the complete elliptic integrals and elementary functions. The details will however be omitted here.

The choked flow state is reached as $b \to \infty$. The limit of ℓ/h as $b \to \infty$ is obviously identical to (39). Furthermore, we derive from (46) the corresponding limit of C_D as

$$C_{D_*} = \frac{2\sin\beta\pi}{\pi U_*}\left(\frac{h}{\ell}\right)\int_0^1\left[\left(\frac{1+\sqrt{1-\zeta^2}}{\zeta}\right)^{2\beta} - \left(\frac{1-\sqrt{1-\zeta^2}}{\zeta}\right)^{2\beta}\right]\frac{\zeta d\zeta}{\zeta^2+a_*^2}$$

$$= \frac{h}{\ell}\left(\frac{1}{U_*} - 1\right)^2 \tag{47}$$

upon integration with appropriate change of variables $(t=(1-\sqrt{1-\zeta^2})/\zeta$ and integrating in the complex t-plane with use of the theorem of residues). This result agrees with (10) which was obtained by using the momentum theorem, as should be expected.

To the other extremity, the unbounded flow limit is obtained as $b \to a$, with the corresponding drag coefficient given by

$$C_{D_o}(\beta,\sigma) = (1+\sigma)\left[1 - \frac{I_-}{I_+}\right] \tag{48}$$

where

$$I_\pm = \int_0^1 \frac{(1\pm\sqrt{1-\zeta^2})^{2\beta}\,\zeta^{1-2\beta}}{(\zeta^2+a^2)^{3/2}}\,d\zeta \quad .$$

This result is shown in Fig. 4 together with two other flow models. The final numerical result of $C_D(\sigma,\beta,\lambda)$ for $\sigma > \sigma_*$ will be presented and discussed in Section 6.

5. Re-entrant Jet Model

The re-entrant jet model has been adopted by Gurevich (1953) to evaluate symmetric cavity flows past a wedge placed in a straight channel. In what follows the general case of a symmetric body of an arbitrary shape is treated by using this model, and the detailed numerical results of the wedge problem are further explored.

The corresponding regions in the z- and f-planes are shown in Fig. 6. Though a parametric plane similar to those of the previous two models (that is, with the body surface and cavity boundaries span the entire real axis of the parametric plane) can also be constructed, the present $\zeta = \xi + i\eta$ plane has certain simplifications. The upper half strip of the f-plane is mapped into the second quadrant of the ζ-plane by the transformation

$$\frac{df}{d\zeta} = \frac{A\zeta(\zeta^2-c^2)}{(\zeta^2-a^2)(\zeta^2-b^2)} \quad . \tag{49}$$

where A is a positive real constant. By this formula f can be continued analytically into the entire ζ-plane (by virtue of $\psi = \mathrm{Im} f = 0$ on $\xi = 0$). From the local singular behavior of f at $\zeta = a, b,$ and ∞ it follows that

$$Uh = \pi A(c^2-a^2)/(b^2-a^2) \quad , \tag{50}$$

$$Vh = \pi A(c^2-b^2)/(b^2-a^2) \quad , \tag{51}$$

$$\ell_j = \pi A \quad . \tag{52}$$

Condition (51) assures that the flow at the downstream channel is simply covered. From (50) and (51) it also follows that

$$V/U = (c^2-b^2)/(c^2-a^2) \quad . \tag{53}$$

From equations (50) - (52) follows also the continuity condition $(U-V)h=\ell j$.

The boundary conditions of $\omega = \tau + i\theta$ are

$$\begin{aligned} \theta^+(\xi) = \theta(\xi,+0) &= -\pi && (\xi < -c) \\ &= 0 && (-c < \xi < -1) \\ &= \beta(\xi) && (-1 < \xi < 0) \\ \tau(0,\eta) &= 0 && (\eta > 0) \quad . \end{aligned} \tag{54}$$

The last condition of (54) enables $\omega(\zeta)$ to be analytically continued into the first quadrant of the ζ-plane by $\omega(-\bar{\zeta}) = -\overline{\omega(\zeta)}$, that is, τ is odd and θ is even in ξ. ($\omega(\zeta)$ can further be continued into the lower half ζ-plane by $\omega(\bar{\zeta}) = \overline{\omega(\zeta)}$ so that θ is odd in η. The lower half flow field then corresponds to the fourth quadrant of the ζ-plane.) After this continuation, θ is prescribed as an even function of ξ, for the entire ξ-axis. The solution $\omega(\zeta)$ is then given by the Poisson integral

$$\omega(\zeta) = \frac{1}{\pi}\int_{-\infty}^{\infty} \frac{\theta^+(\xi)d\xi}{\xi-\zeta} = \log\frac{c-\zeta}{c+\zeta} + \frac{1}{\pi}\int_{-1}^{1}\frac{\beta(\xi)d\xi}{\xi-\zeta} \quad . \tag{55}$$

Hence,

$$w(\zeta) = e^{-\omega} = \left(\frac{c+\zeta}{c-\zeta}\right)e^{-\Omega(\zeta)} \quad , \qquad \Omega(\zeta) = \frac{1}{\pi}\int_{-1}^{1}\frac{\beta(\xi)d\xi}{\xi-\zeta} \quad . \tag{56}$$

The boundary conditions of ω at point A and B require that

$$U = \left(\frac{c-a}{c+a}\right)e^{-\Omega(-a)} \quad , \qquad V = \left(\frac{c-b}{c+b}\right)e^{-\Omega(-b)} \quad . \tag{57}$$

Upon substituting the above U, V into (53), there results

$$(c+b)/(c+a) = \exp\left\{\frac{1}{2}\left[\Omega(-a)-\Omega(-b)\right]\right\} \tag{58}$$

from which it is convenient to determine c as a function of a, b; c will be regarded as such in the sequel.

The physical plane is given by

$$z(\zeta) = \int_{-1}^{\zeta} \frac{1}{w} \frac{df}{d\zeta} = A \int_{-1}^{\zeta} e^{\Omega(\zeta)} \nu(\zeta; a, b) d\zeta \quad , \quad \nu = \frac{(-\zeta)(\zeta - c)^2}{(\zeta^2 - a^2)(\zeta^2 - b^2)} . \tag{59}$$

The half-base chord is $\ell/2 = \text{Im}\, z(0)$, and hence, upon using (50),

$$\frac{\ell}{h} = \frac{2U}{\pi} \frac{b^2 - a^2}{c^2 - a^2} \text{Im} \int_{-1}^{0} e^{\Omega(\zeta)} \nu(\zeta; a, b) d\zeta \quad . \tag{60}$$

The arc length s measured from E along ED is

$$s(\xi) = A \int_{-1}^{\xi} e^{\Gamma(\xi)} \nu(\xi; a, b) d\xi \quad , \quad \Gamma(\xi) = \frac{1}{\pi} \oint_{-1}^{1} \frac{\beta(t) dt}{t - \xi} \quad . \tag{61}$$

For the inverse problem with prescribed $P'[\beta(\xi), a, b]$, c is determined by (58), U by (57), ℓ/h by (60) and $s(\xi)$ by (61). Solution of the direct problem $P[\beta(s), \sigma, \ell/h]$ can proceed along the same method as described earlier for the other two models; it is however more complicated than the previous two models since this solution contains an extra parameter in the first place.

The drag coefficient has been derived for the general asymmetric flows by applying the momentum theorem (see (17)). For the present problem, $q_c = 1$, $\gamma = 0$,

$$C_D = \frac{D}{\frac{1}{2}\rho U^2 \ell} = \frac{h}{\ell} \left(1 - \frac{V}{U}\right)\left(1 + \frac{V+2}{U}\right) . \tag{62}$$

5.1 Symmetric wedge

For a symmetric wedge of half vertex angle $\beta\pi$, Ω can be integrated to yield

$$\Omega(\zeta) = \beta \log \frac{\zeta - 1}{\zeta + 1} \tag{63}$$

which is defined in the ζ-plane cut along the ξ-axis from $\zeta = -1$ to 1 so that $\Omega \to -2\beta/\zeta$ as $|\zeta| \to \infty$. Hence, by (57),

$$U = \left(\frac{c-a}{c+a}\right)\left(\frac{a-1}{a+1}\right)^{\beta} \quad , \quad V = \left(\frac{c-b}{c+b}\right)\left(\frac{b-1}{b+1}\right)^{\beta} \quad , \tag{64}$$

and (58) becomes

$$c = \frac{\kappa b - a}{1-\kappa} \quad , \quad \kappa \equiv \left(\frac{a-1}{a+1}\right)^{\beta/2} \left(\frac{b+1}{b-1}\right)^{\beta/2} \quad . \tag{65}$$

Upon substituting (63) in (60),

$$\frac{\ell}{h} = \frac{2U}{\pi} (\sin \beta\pi) \frac{b^2 - a^2}{c^2 - a^2} \int_0^1 \left(\frac{1+\zeta}{1-\zeta}\right)^{\beta} \frac{\zeta(\zeta + c)^2}{(\zeta^2 - a^2)(\zeta^2 - b^2)} \, d\zeta \quad . \tag{66}$$

Equation (64) - (66) determine U, ℓ/h in terms of a, b, and vice versa.

The choked flow state is approached as $c \to \infty$, and $b \to \infty$. When both b and c are large compared with a, we deduce from (65) the relation

$$\frac{c}{b} = \frac{\kappa}{1-\kappa}\left[1 + 0\left(\frac{a}{b}\right)\right] \quad \text{with} \quad \kappa \simeq \left(\frac{a_* - 1}{a_* + 1}\right)^{\beta/2} \quad . \tag{67}$$

Using (67) in (64), we obtain for $b \gg a$,

$$U_* = \kappa^2 \quad , \quad V_* = 2\kappa - 1 \quad . \tag{68}$$

The corresponding limit of ℓ/h is simply

$$\frac{\ell}{h} = \frac{2U_*}{\pi} \sin \beta\pi \int_0^1 \left(\frac{1+\zeta}{1-\zeta}\right)^{\beta} \frac{\zeta \, d\zeta}{a_*^2 - \zeta^2} \quad . \tag{69}$$

By substituting (68) in (62), we find

$$C_{D_*} = \frac{h}{\ell}\left(\frac{1}{U_*} - 1\right)^2 \tag{70}$$

which is in agreement with the previous two flow models. From the requirement $U_* < 1$ and $V_* > 0$ it follows that κ must lie in the range $\frac{1}{2} < \kappa < 1$, and hence $a_* > (1+\gamma)/(1-\gamma)$, $\gamma = 2^{-2/\beta}$.

The unbounded flow limit can be derived by letting $b \to a$, and by applying l'Hospital's rule to (65), giving

$$c = \frac{1}{\beta}\,(a^2-1)-a \quad , \tag{71}$$

hence by (64),

$$U = \frac{a^2-1-2a\beta}{(a-1)^{1-\beta}(a+1)^{1+\beta}} \quad . \tag{72}$$

We further obtain for the drag coefficient,

$$C_{D_o} = \frac{\pi(1+U)}{aU^2 \sin\beta\pi}\left(\beta\,\frac{c^2-a^2}{a^2-1} - C\right)\frac{I}{I} = \frac{\pi(1+U)}{U^2 \sin\beta\pi}\,\frac{1}{I} \tag{73}$$

upon using (71), where

$$I = \int_o^1 \left(\frac{1+\zeta}{1-\zeta}\right)^\beta \frac{\zeta(\zeta+c)^2}{(\zeta^2-a^2)^2}\,d\zeta \quad . \tag{74}$$

This result of C_{D_o} is shown in Fig. 4 with the previous two flow models.

6. Discussion and Analysis of the Results

From Fig. 4 we see clearly that insofar as the drag coefficient C_{D_o} for unbounded flows is concerned, the discrepancy between the three cavity flow models considered here is rather insignificant for moderate and large wedge angles (say $\beta\pi > 45°$), but becomes quite appreciable for small values of β.

For sufficiently large β (say $\beta\pi > 60°$), the dependence of C_{D_o} on σ can be approximated by the relationship

$$C_{D_o}(\beta,\sigma) = (1 + \sigma + \epsilon(\beta)\sigma^2)\,C_{D_o}(\beta, 0) \tag{75}$$

in which ϵ is a number very small compared with unity. Take the flat plate for example ($\beta = 1/2$), $\epsilon = [8(\pi+4)]^{-1}$ for both the Riabouchinsky and the re-entrant jet models and $\epsilon = [6(\pi+4)]^{-1}$ for the open-wake model (see Wu(1956)) which will make (75) a good approximation for $\sigma < 1$, in which range the nonlinear term $\epsilon\sigma^2$ modifies the result by at most 0.8%. Blunt bodies of arbitrary shape generally also satisfy the above relationship. The slightly less accurate dependence of $C_{D_o}(\sigma,\beta)$ on σ, with the linear factor $(1+\sigma)$, is notorious.

For smaller values of β, the general trend is that, for fixed β and σ, the open wake model yields the largest C_{D_o} whereas the re-entrant jet model gives the smallest C_{D_o} of the three models. Furthermore, when β is very small ($\beta < 1/18$, or $\beta\pi < 10°$), the open wake model is noted to posses the following simple relationship (see Fig. 4)

$$C_{D_o}(\beta,\sigma) \simeq \sigma \qquad (\sigma > (\beta\pi)^{\frac{1}{2}}, \quad \beta \ll 1) \tag{76}$$

which is accurate to a high degree. This finding thus indicates that the cavity flow approximation of Betz (1930), namely $C_{D_o}(\beta, \sigma) = C_{D_o}(\beta, o) + \sigma$, though too crude in general, becomes nevertheless a fairly good approximation in the above range of the parameters σ and β. This feature of the open wake model and the fact that the differences between these flow models becomes increasingly more appreciable with decreasing wedge angle (or, generally, decreasing body thickness ratio) have not been widely known.

We proceed to discuss the theoretical results of the wall effect for symmetric wedges. For the cavitation number σ greater than the blockage constant σ_*, with the cavity finite in length, the drag coefficient $C_D(\beta, \sigma, \lambda)$ has been calculated from (30), (35) - (37) for the open wake mode, from (45), (46) for the Riabouchinsky model, and from (62), (64) - (66) for the re-entrant jet model. In order to improve the rate of convergence of the numerical integration, certain transformations of the variables of integration have been administered, which are desirable particularly for β and σ small when the convergence of the original integrals is relatively slow. The numerical computation has been carried out with an IBM-360 machine, using the straightforward iteration scheme described earlier for the direct problem. Convergence of the iterations has been satisfactory, the errors allowed are less than 10^{-6}. The final results of the numerical solutions are shown in Figs. 7 - 11, from which the percentage drag reduction due to the wall effect is deduced and presented in Fig. 12a and 12b.

From these numerical results we note the following important features of the wall effects in cavity flows. First, the wall effects for straight channels always result in a lower drag coefficient than for an unbounded flow at the same cavitation number. This is physically obvious since the lateral constraints of the tunnel walls must make the flow velocity somewhat higher, and hence the pressure lower, than their corresponding values for unbounded flows over the wetted body surface away from the stagnation point, provided the comparison is made for the same cavitation number (or the same base under-pressure coefficient).

Another remarkable feature of the results is that the wall effect, measured by the percentage drag reduction at fixed σ and ℓ/h, actually increases with decreasing wedge angle - - a property in common to all three flow models employed. This would imply a general conclusion that wall effects are more significant for thinner bodies in cavity flows, other conditions being equal. At a first glance, such a statement may even contradict one's intuition. However, it is to be noted as physically plausible that the pressure reduction over the wetted side of a thin body may be felt over a longer stretch than for blunt bodies. Another possible reason is that the curvature singularity of the cavity boundary at the separation becomes weaker as the body thickness ratio decreases, causing a greater pressure reduction on the wetted side.

A third feature of interest is that the drag reduction (absolute difference) is very much insensitive to $\sigma (> \sigma_*)$ for fixed β and λ. This feature is again common to all three flow models considered. Furthermore, it is to be noted that the wall effects predicted by the open wake model are considerably stronger than the other two models. This interesting finding and the differences between these flow models in the case of unbounded flows past thin bodies strongly suggest that the decisive support must come from further precise experimental investigations.

II. LIFTING CAVITY FLOWS

7. General Formulation of Choked Lifting Flows

As a typical case, we consider the plane flow past an arbitrary curved obstacle held at an arbitrary location in the tunnel, characterized by the distance h_D between the detachment point D and the tunnel wall, and by the orientation of the body, as shown in Fig. 13. In fact, to be general, we may also admit curved tunnel walls in our formulation so long as the bounding walls become asymptotically straight at both terminals so that uniform conditions can be prescribed at up and downstream infinities. Thus, the geometric inclination of the solid surface will be denoted by $\beta(s)$ along the body surface and by $\alpha(s)$ along the tunnel walls, both as functions of the arc length s, measured along the surface in the sense of increasing x. The entire flow region in the complex potential f-plane, with $f = 0$ at the stagnation point E, lies in a strip bounded by $\psi = \psi_1 = Uh_1 = Vd_1$ and $\psi = -\psi_2$, where $\psi_2 = Uh_2 = Vd_2$. We next map this f-strip into the upper half of the parametric ζ-plane, with $\zeta_D = -1$, $\zeta_{D'} = 1$, $\zeta_E = \infty$, by the transformation

$$\frac{df}{d\zeta} = \frac{-A}{(\zeta-a)(\zeta-b)(\zeta-b')} , \tag{77}$$

where A is a real constant, $\zeta = a, b, b'$ are the respective image points of the upstream infinity A, upper jet B and lower jet B'. The jumps in ψ across A, B, B' provide the relations

$$Uh_1 = Vd_1 = \frac{\pi A}{(a-b)(b'-b)} , \quad Uh_2 = Vd_2 = \frac{\pi A}{(b'-a)(b'-b)} . \tag{78}$$

In terms of the ratio

$$\gamma = h_1/(h_1+h_2) \equiv h_1/h = (b'-a)/(b'-b) \quad , \tag{79}$$

$$b' = (a-\gamma b)/(1-\gamma) \quad . \tag{80}$$

Adding the two equations in (78), we have

$$Uh = V(d_1+d_2) = \frac{\pi A}{(a-b)(b'-a)} = \frac{\pi A(1-\gamma)}{\gamma(a-b)^2} \quad . \tag{81}$$

It is convenient to decompose the logarithmic hodograph variable

$$\omega(\zeta) = \log \frac{V}{w} = \tau + i\theta \tag{82}$$

into two parts

$$\omega = \omega_o+\omega_1 \quad , \quad \omega_o = \tau_o+i\theta_o \quad , \quad \omega_1 = \tau_1 + i\theta_1 \quad , \tag{83}$$

such that the boundary conditions of ω assume the following decomposition (with $\zeta = \xi + i\eta$)

$$\theta_o = \pi+\beta(\xi) \quad , \qquad \theta_1 = 0 \qquad (\xi < -1, \ \eta = 0) \quad , \tag{84a}$$

$$\tau_o = 0 \quad , \qquad \tau_1 = 0 \qquad (-1 < \xi < b \ , \ b' < \xi < 1, \ \eta = 0) \quad , \tag{84b}$$

$$\tau_o = 0 \quad , \qquad \theta_1 = \alpha(\xi)-\theta_o(\xi) \ (b < \xi < b', \ \eta = 0) \quad , \tag{84c}$$

$$\theta_o = \beta(\xi) \quad , \qquad \theta_1 = 0 \qquad (\xi > 1, \ \eta = 0) \quad . \tag{84d}$$

In the above conditions, the inclination angles α and β are regarded as functions of ξ; and in (84c), $\theta_o(\xi)$ is known when the solution $\omega_o(\zeta)$ is obtained. The problem of $\omega_o(\zeta)$ is the same as the unbounded flow case which has been solved by Wu and Wang (1964a), and the solution is

$$\omega_o = \log[\zeta+(\zeta^2-1)^{\frac{1}{2}}] - \frac{1}{\pi}(\zeta^2-1)^{\frac{1}{2}}\left(\int_{-\infty}^{-1} - \int_{1}^{\infty}\right)\frac{\beta(\xi)d\xi}{(\xi-\zeta)(\xi^2-1)^{\frac{1}{2}}} \quad . \tag{85}$$

The problem of ω_1 can be expressed as a Hilbert boundary problem,* its solution can be shown to be

$$\omega_1(\zeta) = -\frac{1}{\pi}[(\zeta-b)(\zeta-b')(\zeta^2-1)]^{\frac{1}{2}}\int_b^{b'}\frac{[\alpha(\xi)-\theta_o(\xi)]d\xi}{(\xi-\zeta)[(\xi-b)(b'-\xi)(1-\xi^2)]^{\frac{1}{2}}} \quad . \tag{86}$$

The above expressions of ω_o and ω_1 contain branch points at $\zeta = \pm 1$, b and b'; the branch of $(\zeta^2-1)^{\frac{1}{2}}$ is defined with a branch cut from $-\infty$ to -1 and from $+1$ to ∞, while $(\zeta-b)^{\frac{1}{2}}(\zeta-b')^{\frac{1}{2}}$ is defined with a cut from b to b', so that $(\zeta^2-1)^{\frac{1}{2}}$ and $[(\zeta-b)(\zeta-b')]^{\frac{1}{2}}$ both tend to ζ as $|\zeta| \to \infty$ in the upper half plane. By studying the analytical behavior of these integral representations it can be shown† that $\omega = \omega_o + \omega_1$ is continuous in the neighborhood of $\zeta = \pm 1$, b, b' and for finite ζ in the upper half ζ-plane. Near the stagnation point E or $\zeta = \infty$, however, the local conformal behavior requires that ω behaves like $\log\zeta$ as $|\zeta| \to \infty$; this behavior is exhibited by the first term of ω_o, which is not to be changed by the added term ω_1 representing the effect of wall. On the other hand, (86) shows that $\omega_1(\zeta) = O(|\zeta|)$ as $|\zeta| \to \infty$ unless

$$\int_b^{b'}\frac{[\alpha(\xi)-\theta_o(\xi)]d\xi}{[(\xi-b)(b'-\xi)(1-\xi^2)]^{\frac{1}{2}}} = 0 \quad , \tag{87}$$

---

*See, e.g. Muskhelishvili: Singular Integral Equation (1953), pp. 235 - 8.

†See, e.g. by the method discussed by Muskhelishvili: Singular Integral Equation (1953), pp. 235 - 8.

in which case ω_1 is bounded as $|\zeta| \to \infty$. We therefore enforce condition (87) on the solution.

At the upstream infinity, as $\zeta \to a$, the present solution $\omega = \omega_o + \omega_1$ has its imaginary part $\theta(a)$ satisfying automatically the condition on flow inclination, while its real part gives

$$\log \frac{V}{U} = \frac{1}{2}\log(1+\sigma_*) = \tau(a) = \frac{1}{\pi}\int_b^{b'} \frac{[(a-b)(b'-a)(1-a^2)]^{\frac{1}{2}}}{[(\xi-b)(b'-\xi)(1-\xi^2)]^{\frac{1}{2}}} \frac{\alpha(\xi)-\theta_o(\xi)}{\xi-a} d\xi \tag{88}$$

in which the integral takes its Cauchy principal value. This relationship provides another condition on the flow parameters.

The physical z-plane is given by the integration

$$z(\zeta) = \int_{-1}^{\zeta} \frac{1}{w}\frac{df}{d\zeta}\, d\zeta = \frac{1}{V}\int_{-1}^{\zeta} e^{\omega(\zeta)} \frac{df}{d\zeta}\, d\zeta \quad (\eta = \operatorname{Im}\zeta \geqslant 0) \quad , \tag{89}$$

and the arc length measured along the body surface from point D is

$$s(\xi) = \frac{1}{V}\int_{-1}^{\xi} e^{\tau(\xi)} \frac{df}{d\xi}\, d\xi \qquad (|\xi| > 1 \quad , \quad \eta = 0) \quad . \tag{90}$$

In particular, the total wetted arc length is

$$s(1) = \frac{1}{V}\left(\int_{-1}^{-\infty} + \int_{\infty}^{1}\right) e^{\tau(\xi)} \frac{df}{d\xi}\, d\xi = S \quad . \tag{91}$$

Furthermore, the distance of point A from the asymptote of the upper wall far downstream is

$$h_D = d_1 + \operatorname{Im}[e^{-i\alpha_o}(z_B - z_D)] = d_1 - \frac{A}{V}\int_{-1}^{b} \frac{\sin(\theta(\xi)-\alpha_o)d\xi}{(\xi-a)(\xi-b)(\xi-b')} \tag{92}$$

The above integral is regular since $\theta(\xi) = \alpha_o$ at $\xi = a$, b and b'

Finally, we introduce $\tilde{z} = \tilde{x} + i\tilde{y}$ by rotation $\tilde{z} = ze^{-i\alpha_o}$, so that the $\tilde{x}$-axis is parallel to the flow far up and downstream. Then on the upper and lower walls

$$\tilde{y}_+(\xi) = d_1 - \frac{A}{V}\int_{-1}^{\xi} \frac{\sin(\theta(\xi)-\alpha_o)d\xi}{(\xi-a)(\xi-b)(\xi-b')} \qquad (b < \xi < a) \ , \tag{93}$$

$$\tilde{y}_-(\xi) = d_1 - h - \frac{A}{V}\int_{-1}^{\xi} \frac{\sin(\theta(\xi)-\alpha_o)d\xi}{(\xi-a)(\xi-b)(\xi-b')} \quad (a < \xi < b') \ . \tag{94}$$

In general this problem involves four independent parameters, say $\sigma_*(= V^2/U^2-1)$, $\gamma = h_1/h$, a and b (then b' is given by Eq. (80), A by (81) for known U and h, and $V = U(1+\sigma_*)^{\frac{1}{2}}$). For the determination of these four parameters there correspond four equations: (87), (88), (91), (92). Consequently, the inverse problem, with prescribed $\alpha(\xi)$ and $\beta(\xi)$, is completely solved. However, for physical problems when α and β are given as functions of arc length s, it is further necessary to satisfy the integral functional equations (90), (93) and (94). The integral iteration method, or the approximate scheme introduced by Wu and Wang (1964a, b) are useful for computing the solution of this problem.

The simple case of an inclined flat plate at the choking condition in a straight channel has been investigated by Ai (1965), using the present formulation.

Shair et al (1963) showed experimentally that the stability of the steady laminar wake behind a circular cylinder is strongly influenced by the proximity of the tunnel walls.

8. Cavity Flow past an Inclined Flat Plate in Straight Channel

As a simple representative case, we now evaluate the plane flow, with a finite cavity formation, past a flat plate hydrofoil centered in a straight channel. The open wake model with a straight dissipation wake will be adopted to represent the actual flow having a finite cavity. This theoretical model was first applied by Wu (1956) to unbounded lifting flows, yielding satisfactory predictions of the hydrodynamic force coefficients for bodies of small curvatures. For the present problem, the corresponding regions in the z-, f-, and ω-planes are shown together with the parametric ζ-plane in Fig. 14.

The transformation between the f- and ζ-planes is again given by (77) and relationships (78) - (81) still remain valid for the present problem. The flow field occupies a polygonal region in the ω-plane, which can be mapped into the upper half ζ-plane by

$$\omega(\zeta) = \int_1^{\zeta} \frac{(\zeta - m)d\zeta}{[(\zeta^2-1)(\zeta-c)(\zeta-c')]^{\frac{1}{2}}} \tag{95}$$

in which the coefficient of multiplier and constant of integration have been determined to satisfy the conditions at the stagnation point $(\zeta = \infty)$ and at the trailing edge $(\zeta = 1)$. The point $\zeta = m$ on the real axis is the image of the point M on the lower tunnel wall at which the flow velocity along the wall reaches a minimum (for positive incidence α as shown). The function $[(\zeta^2-1)(\zeta-c)(\zeta-c')]^{\frac{1}{2}}$ is analytic in the ζ-plane with branch cuts from $\zeta = -\infty$ to -1, from $\zeta = c$ to c', and from $\zeta = 1$ to $+\infty$ along the real axis so that this function tends to ζ^2 as $|\zeta| \to \infty$ in the upper half plane. There are several conditions on $\omega(\zeta)$. The present flow model requires that $\omega(c) = \omega(c') = i\alpha$, hence

$$\int_{c}^{c'} \frac{(\zeta - m)d\zeta}{[(1-\zeta^2)(\zeta - c)(c' - \zeta)]^{\frac{1}{2}}} = 0 \quad , \tag{96}$$

and

$$\int_{c'}^{1} \frac{(\zeta - m)d\zeta}{[(1-\zeta^2)(\zeta - c)(\zeta - c')]^{\frac{1}{2}}} = \alpha \quad . \tag{97}$$

At the upstream infinity, $\omega(a) = -\log U + i\alpha$, hence $\omega(a) - \omega(c) = -\log U$, or

$$\int_{c}^{a} \frac{(m - \zeta)d\zeta}{[(1-\zeta^2)(\zeta - c)(c' - \zeta)]^{\frac{1}{2}}} = \log \frac{1}{U} \quad . \tag{98}$$

Furthermore, from the downstream condition $\omega(b) = \omega(b') = -\log V + i\alpha$ it follows

$$\int_{b}^{b'} \frac{(\zeta - m)d\zeta}{[(1-\zeta^2)(\zeta - c)(c' - \zeta)]^{\frac{1}{2}}} = 0 \quad , \tag{99}$$

and

$$\int_{c}^{b} \frac{(m - \zeta)d\zeta}{[(1-\zeta^2)(\zeta - c)(c' - \zeta)]^{\frac{1}{2}}} = \log \frac{1}{V} \quad . \tag{100}$$

The physical plane is given by

$$z(\zeta) = \int_{-1}^{\zeta} e^{\omega(\zeta)} \frac{df}{d\zeta} \, d\zeta \tag{101}$$

from which we deduce the chord length of the plate, $\ell = z(1)$, after using (77) - (81) and effecting partial fraction, as

$$\frac{\ell}{h} = \frac{U}{\pi} \int_{-1}^{1} e^{\omega(\zeta)} \left[\frac{1}{\zeta - a} - \frac{\gamma}{\zeta - b} - \frac{1-\gamma}{\zeta - b'} \right] d\zeta \quad . \tag{102}$$

The distance of the leading edge of the plate from the upper wall is clearly

$$h_L = \mathrm{Im}\{e^{-i\alpha} z(c)\} + d_1$$

which can be written as

$$\frac{h_L}{h} = \frac{U}{\pi} \int_{-1}^{c} \sin(\theta-\alpha)\left[\frac{1}{\zeta - a} - \frac{\gamma}{\zeta - b} - \frac{1-\gamma}{\zeta - b'}\right] d\zeta + \frac{\gamma U}{V} \quad (103a)$$

where

$$\theta(\xi) = \alpha + \int_{\xi}^{c} \frac{(m-\zeta)d\zeta}{[(1-\zeta^2)(c-\zeta)(c'-\zeta)]^{\frac{1}{2}}} \qquad (-1 \leqslant \xi \leqslant c) \quad .$$

(103b)

Alternately, the distance h_o of the mid-chord point of the plate from the upper wall is given by

$$\frac{h_o}{h} = \frac{h_L}{h} + \frac{1}{2}\frac{\ell}{h} \sin\alpha \quad . \qquad (104)$$

When the flat plate is centered in the channel, $h_o/h = 1/2$, as often is the case in water tunnel experiments.

The numerical computation of the solution depends on which parameters are chosen to be independent. The direct problem can be specified by the parameters $P[\alpha, \sigma, \ell/h, h_o/h]$. However, there are various ways of posing an inverse problem by making different choices of the remaining parameters, namely, a, b, b', c, c', m, γ, V. A relatively simple procedure is as follows. First we note that (96) determines explicitly $m = m(c, c')$, and consequently (99) yields $b' = b'(b, c, c')$. Therefore, the inverse problem may be specified by the parameters $P'[a, b, c, c']$. With this choice, γ is determined directly by (80), α by (97), U by (98), V by (100), ℓ/h by (102), and h_L/h by (103).

In the actual execution of numerical computations for the direct problem it is found more convenient to work with the following mixed type problem $P''[\alpha, c, b, \gamma]$. In this problem, with m eliminated by combining (96) and (97), the resulting equation determines $c' = c'(\alpha, c)$ by iteration and then $m = m(\alpha, c)$ by (96). From (99), b' is determined as $b' = b'(\alpha, c, b)$ again by iteration. After a value of γ is chosen, a is derived from (80), then a straighforward computation may be carried out for σ, ℓ/h and h_o/h by (98), (102) and (104), respectively. In order to fix a given value of h_o/h, a simple iteration with respect to γ is necessary for the set of equations, (80), (98), (102) and (104). Finally, the case of a given ℓ/h may be obtained by a cross plotting procedure. To facilitate the numerical integration, the integrals appearing in these formulas have been converted into the Jacobian elliptic functions of the first, second and third kind and the existing numerical program for these functions devised by Ai and Harrison (1964), with accuracy to six figures, has been adopted in the present numerical scheme. The computation has been carried out with an IBM-360 machine at the Booth Computing Center of the California Institute of Technology. A few representative cases are shown in Figs. 15 - 16. These results will be discussed below.

Two limiting cases are reached in this computation. One of them is the choked flow state which is approached as $b \to c$ and $b' \to c'$. In this limit, (99) reduces to (96) and (100) drops out as $V \to 1$. This choked flow case has been treated earlier by Ai (1965) based on a formulation which, as described in the previous section, is somewhat different from the present one. The present numerical result in the choked flow limit is found to agree exactly with that of Ai.

The other limiting case is the unbounded flow which is reached as b, b' and m all tend to a. This unbounded flow case has been evaluated earlier by Wu (1956) whose solution is based on an expansion for small σ. The present exact solution in the limit of unbounded flow is in good agreement with the previous result of Wu (1956) for $\sigma < 1$.

From the final result as shown in Figs. 15 - 16 the following salient features may be noted of the wall effects in lifting cavity flows. Apparently, the results from a flat plate at an angle of attack exhibit a similar general trend of the wall effects as in the pure drag case. Based on the same cavitation number σ, the wall effect in the inviscid flow is found to reduce both the drag and the lift coefficients of the flat plate. Furthermore, the smaller the incidence angle, the more significant becomes the wall effect when measured in terms of the percentage change in lift and drag coefficients. Such a phenomenon should not be too difficult to understand as small changes in a thin cavity above a lifting plate would be expected to have more effect on the forces than changes in a thicker cavity for reasons similar to those given in the pure drag case. A closer examination of the details in the numerical results further indicates that at small incidences, the wall effects actually become slightly more appreciable as the cavity shortens from the choked flow state, in a stretch of $\sigma > \sigma_*$, before they become insensitive to σ for further increase in σ. This refined trend diminishes as the angle of attack α increases. As $\alpha \to \pi/2$, the present result agrees exactly with the pure drag case of a flat plate obtained in Part I, thus providing an independent check of the accuracy of the present numerical computation.

For an inclined flat plate it is obvious that a decrease in lift must accompany a reduction in drag since the resultant force must be normal to the plate. Although it remains to be verified, the same feature of the wall effects is likely to hold for cavitating hydrofoils of small curvature.

References

Ai, D.K. (1966) The wall effect in cavity flows. Trans. ASME, J. Basic Eng. 88D, 132 - 138 (also issued Tech. Rep. E-111-3).

Ai, D.K. and Harrison, Z. L. (1964) A computer method for calculation of the complete and incomplete elliptic integrals of the third kind. Rept. E-110.3, Calif. Inst. of Tech.

Barr, R.A. (1966) An investigation of the cavity flow behind drag discs and supercavitating propellers. M.S. Thesis, Univ. of Maryland.

Birkhoff, G. (1950) Hydrodynamics. Princeton University Press.

Birkhoff, G., Plesset, M. and Simmons, N. (1950) Wall effects in cavity flow I. Quart. Appl. Math. 8, 161 - 168.

Birkhoff, G., Plesset, M. and Simmons, N. (1952) Wall effects in cavity flow II. Quart. Appl. Math. 9, 413 - 421.

Brennen, C. (1969) A numerical solution of axisymmetric cavity flows. To appear in J. Fluid Mech.

Caywood, T.E. (1946) Unpublished.

Cisotti, U. (1922) Idromeccanica Piana. Milano.

Cohen, H. and DiPrima, R.C. (1958) Wall effects in cavitating flows. Proc. Second Symp. on Naval Hydrodynamics. ACR-38, Washington, D.C.,: Govt. Printing Office.

Cohen, H. and Gilbert, R., (1957) Two-dimensional, steady, cavity flow about slender bodies in channels of finite breadth. J. Appl. Mech. 24, 170 - 176.

Cohen, H., Sutherland, C. C., and Tu, Y. (1957) Wall effects in cavitating hydrofoil flow. J. Ship Res. 3, 31 - 40.

Dobay, G.F. (1967) Experimental investigation of wall effect on simple cavity flows. Proc. Symp. Testing Techniques in Ship Cavitation Research. Vol. 1, 175-230, Skipsmodelltanken, Tronheim, Norway.

Fabula, A.G. (1964) Choked flow about vented or cavitating hydrofoils. Trans. ASME, J. Basic Eng. 86D 561 - 568.

Gilbarg, D. (1949) Proc. Nat. Acad. Sci. U.S.A. 35, 609 - 612.

Gilbarg, D. (1960) Jets and Cavities. In "Handbuch der Physik," Vol. IX, 311 - 445. Springer-Verlag, Berlin.

Grove, A.S. Shair, F.H., Petersen, E.E. and Acrivos, A. (1964) An experimental investigation of the steady separated flow past a circular cylinder. J. Fluid Mech. 19, 60 - 80.

Gurevich, M.I. (1963) Proc. A.I. Mikoyan, Moscow Tech. Inst. of Fis. Ind. Econ. V.

Meijer, M.C. (1967) Pressure measurement on flapped hydrofoils in cavity flows and wake flows. J. Ship Res. 11, 170 - 189.

Morgan, W.B. (1966) The testing of hydrofoils and propellers for fully-cavitating or ventilated operation. Proc. 11th ITTC 202-218, Tokyo, Japan.

Valcovici, V. (1913) Über discontinuierliche Flüssigkeitsbewegungen mit zwei freien Strahlen, Thesis, Gottingen.

Villat, H. (1914) Sur la validité des solutions de certains problèmes d'hydrodynamique. J. de Math. (6), 10, 231 - 290.

Waid, R. L. (1968) Cavity Flows - - Part of Report on Cavitation. Proc. 15th ATTC, National Res. Conc. Ottawa, Canada.

Wang, D. P., and Wu, T. Y. (1963) Small-time behavior of unsteady cavity flows. Arch. Rat. Mech. and Anal. 14, 127 - 152.

Wu, T. Y. (1956) Discussion of paper by Gilbarg, D., Proc. 1st Symp. on Naval Hydrodynamics, Nat. Acad. Sci - Nat. Res. Counc. Publ. 515, p. 293 - 294.

Wu, T. Y. (1956) A free streamline theory for two-dimensional fully cavitated hydrofoils. J. Math. Phys. 35, 236 - 265.

Wu, T. Y. (1962) A wake model for free streamline flow theory, Part I. Fully and partially developed wake flows and cavity flows past an oblique flat plate. J. Fluid Mech. 13, 161 - 181.

Wu, T. Y. (1968) Inviscid Cavity and Wake Flows, article in "Basic Developments in Fluid Dynamics" (M. Holt, ed.) Academic Press, New York.

Wu, T. Y., and Wang, D. P. (1964a) A wake model for free-streamline flow theory, Part 2. Cavity flows past obstacles of arbitrary profile. J. Fluid Mech. 18, 65 - 93.

Wu, T. Y. and Wang, D. P. (1964b) An approximate numerical scheme for the theory of cavity flows past obstacles of arbitrary profile. Trans. ASME, J. Basic Eng. 86D, 556 - 560.

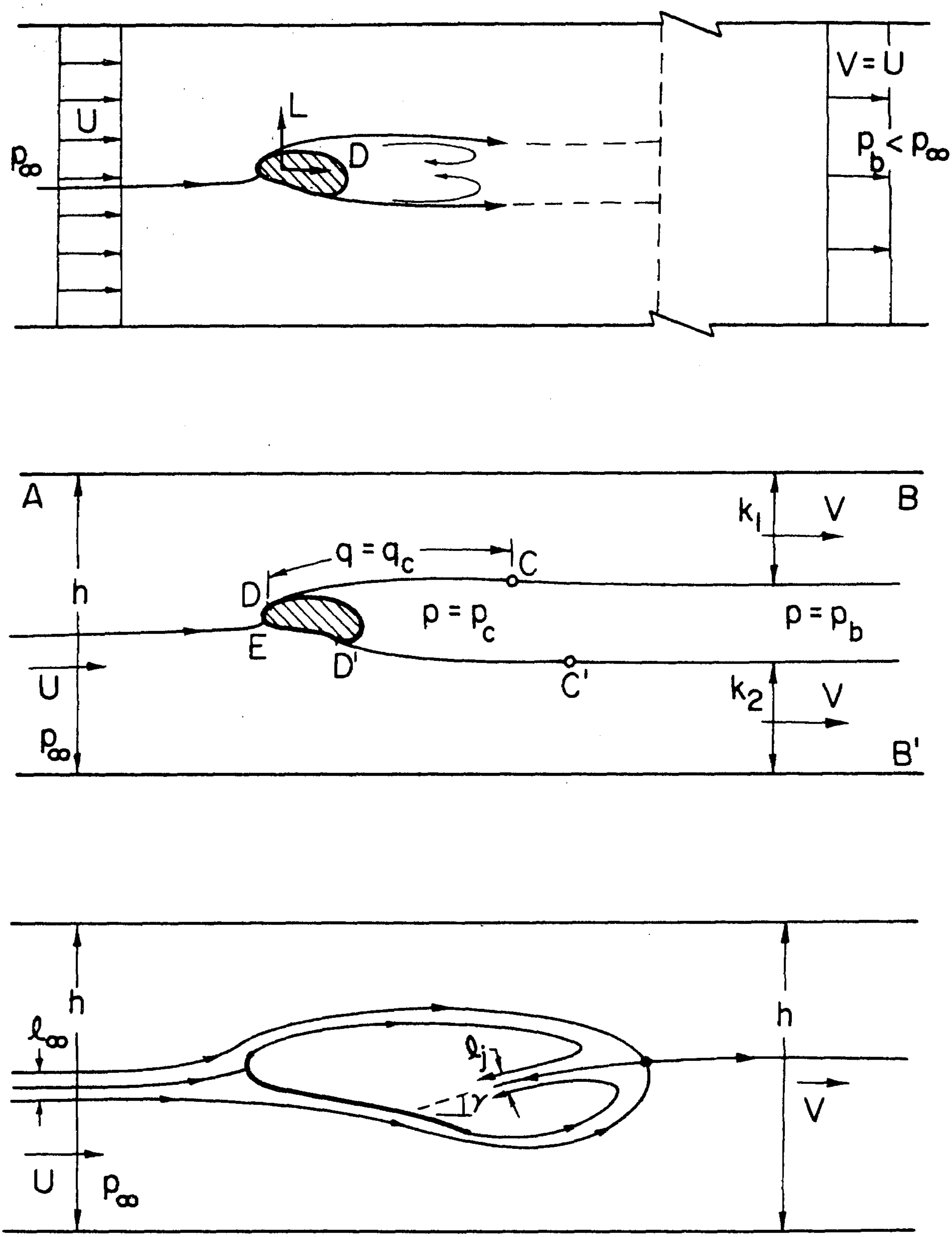

Fig. 1 Momentum considerations for cavity and wake flows.

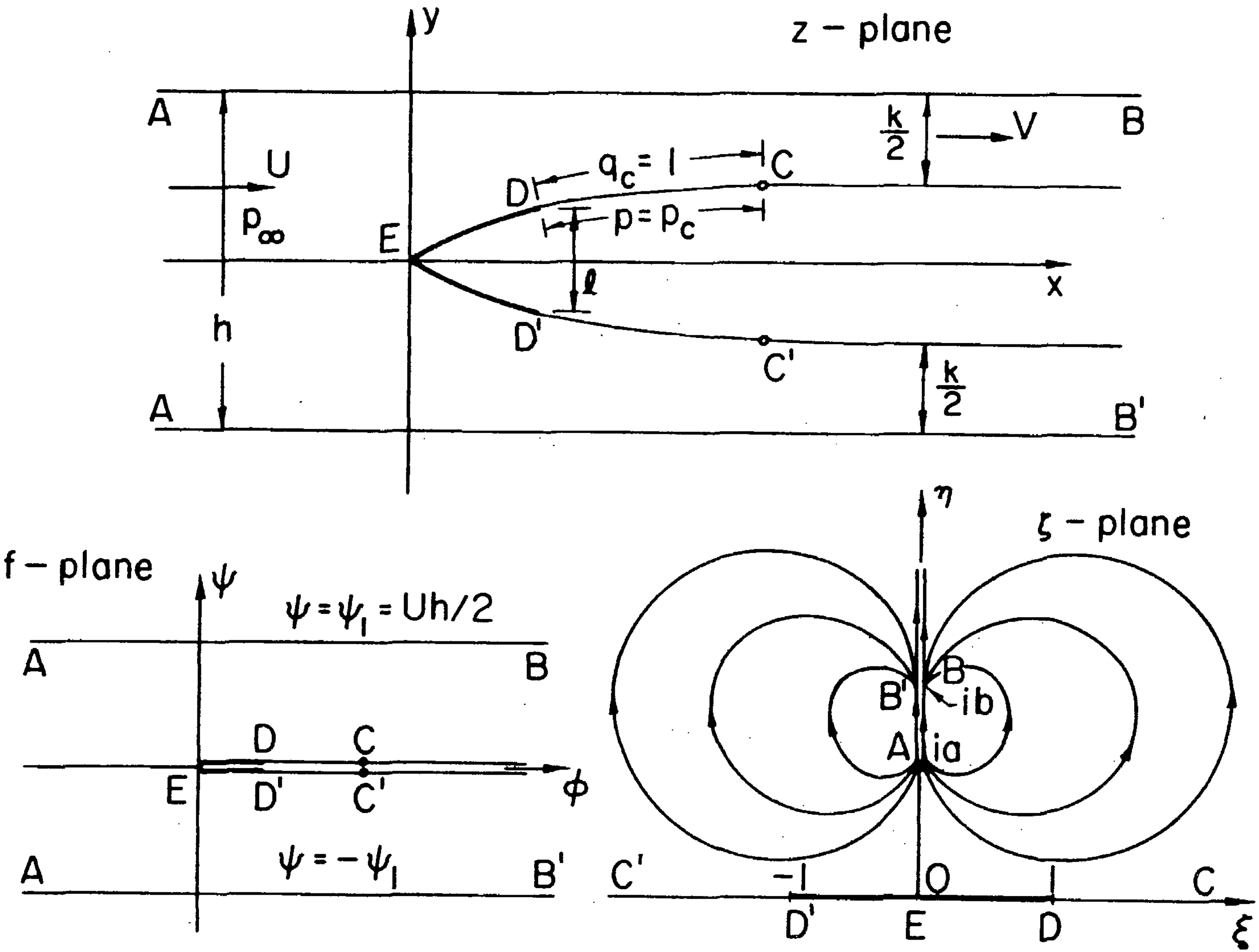

Fig. 2 The open wake model for pure drag cavity flows in a channel.

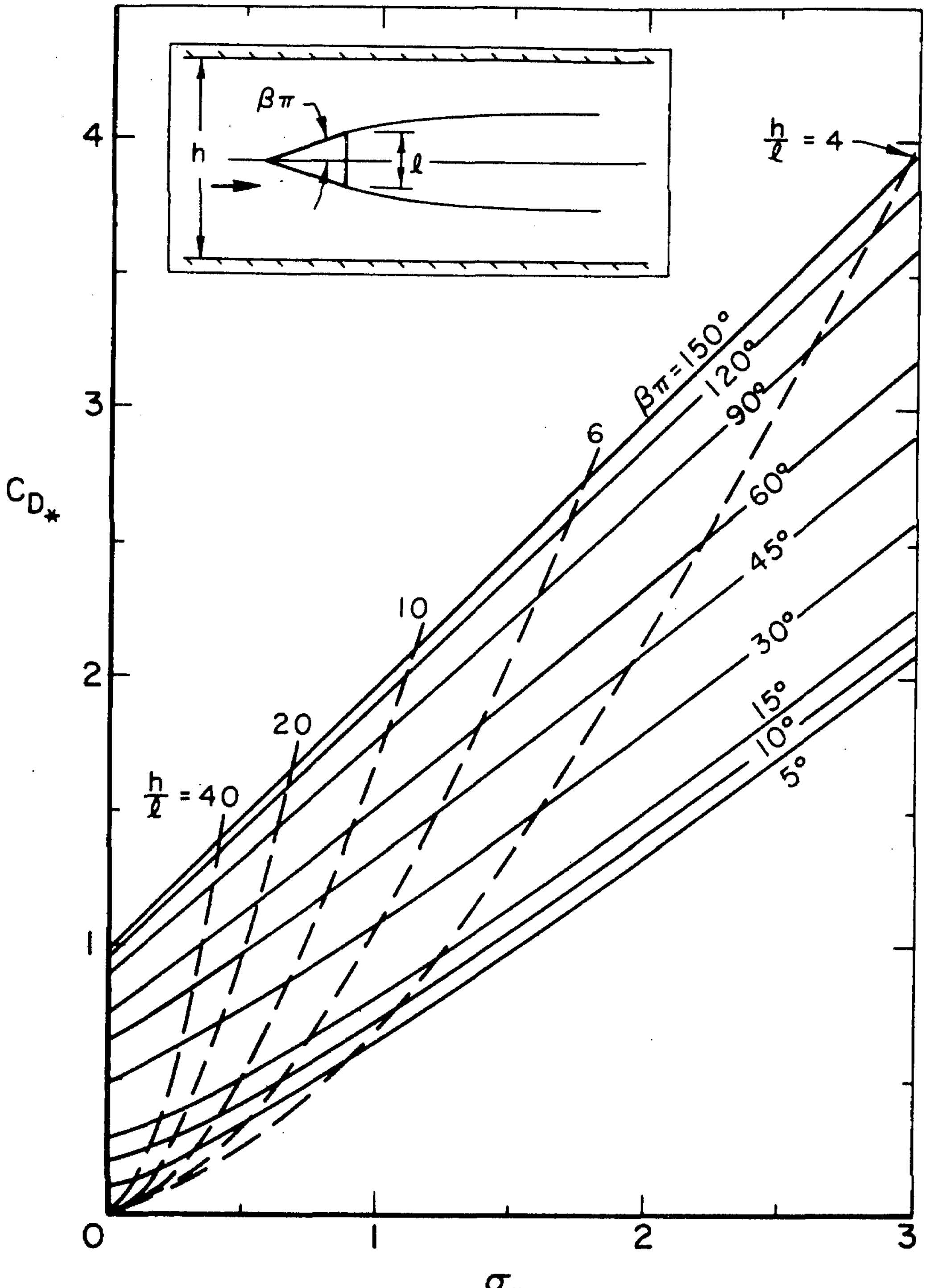

Fig. 3a Choked flow drag $C_{D_*}(\sigma_*, \beta, \ell h)$ of wedges versus the choking cavitation number σ_*. Cavity is finite in length for $\sigma > \sigma_*(\beta, \ell h)$.

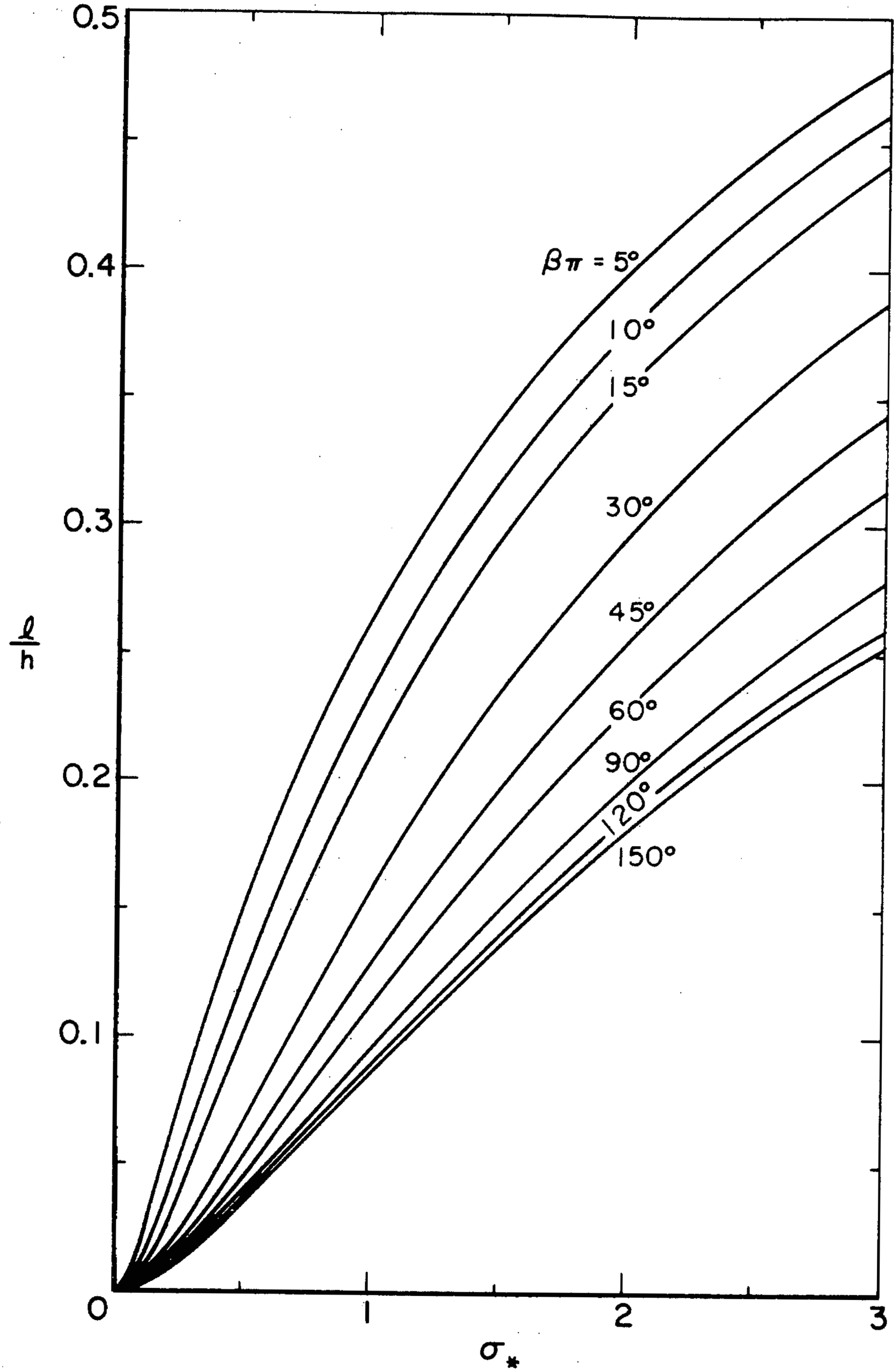

Fig. 3b Choked channel width versus σ_*.

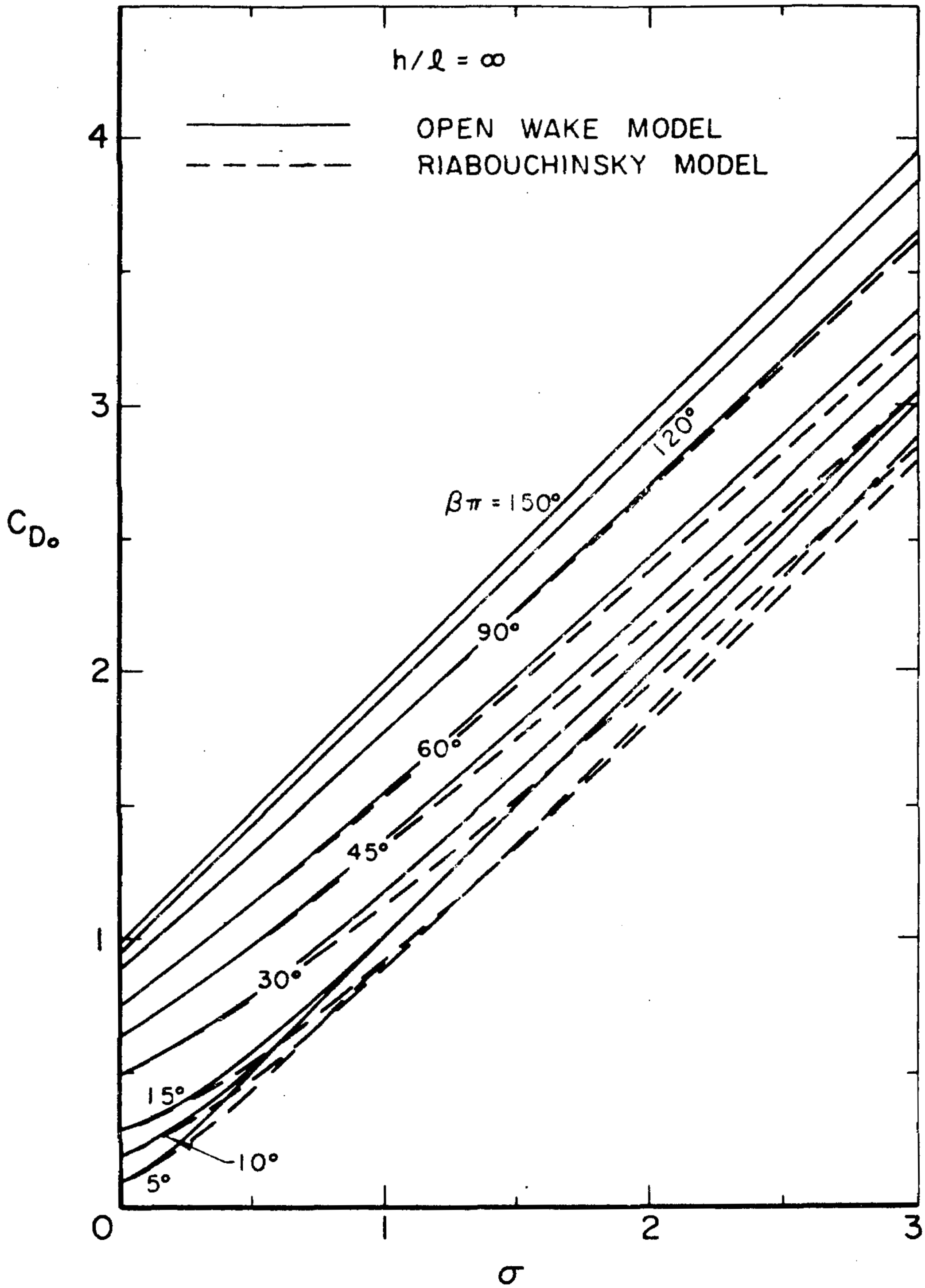

Fig. 4 Drag coefficients of wedges in unbounded flow based on different theoretical models.

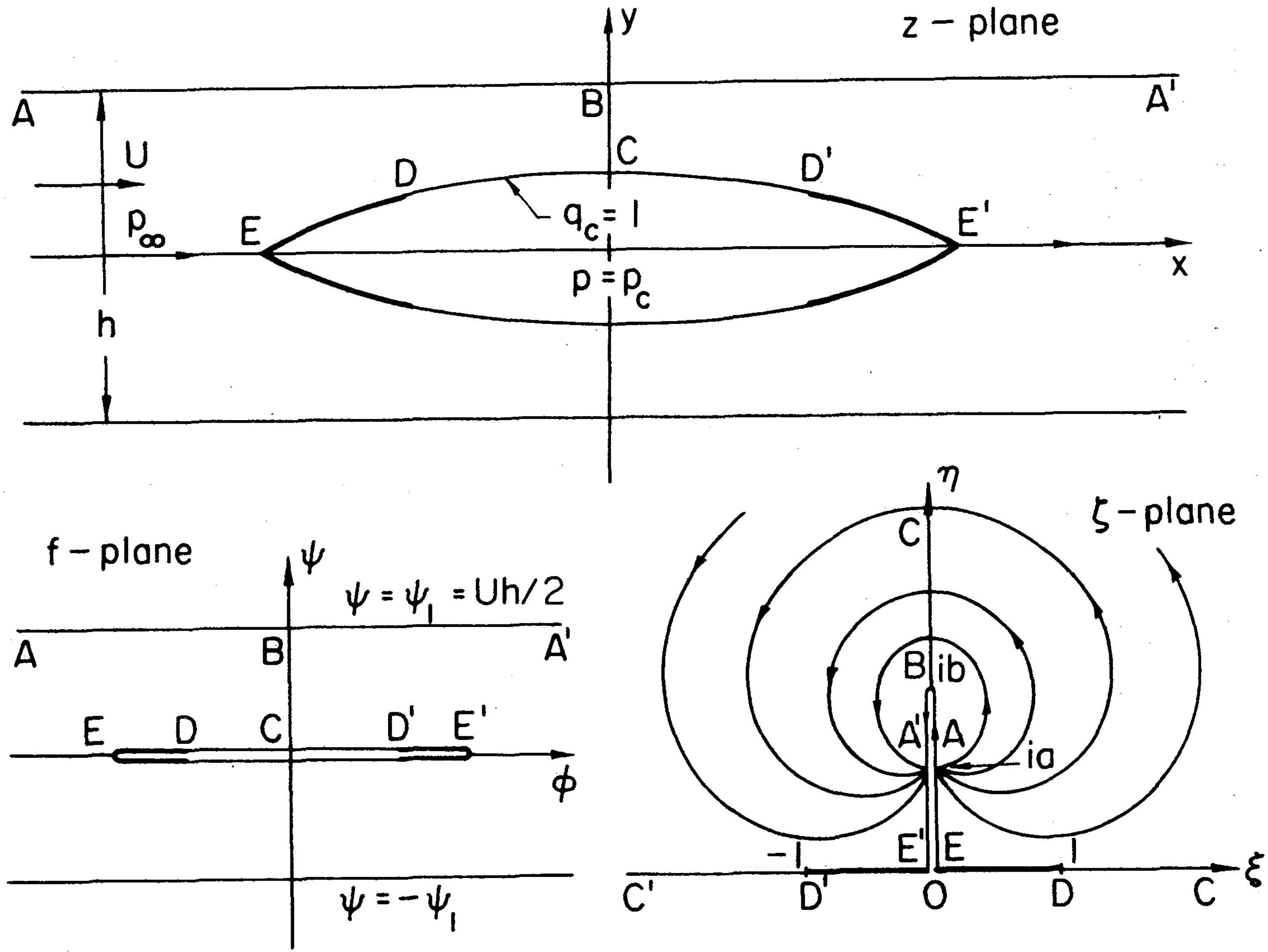

Fig. 5 The Riabouchinsky model for pure drag cavity flows in a channel.

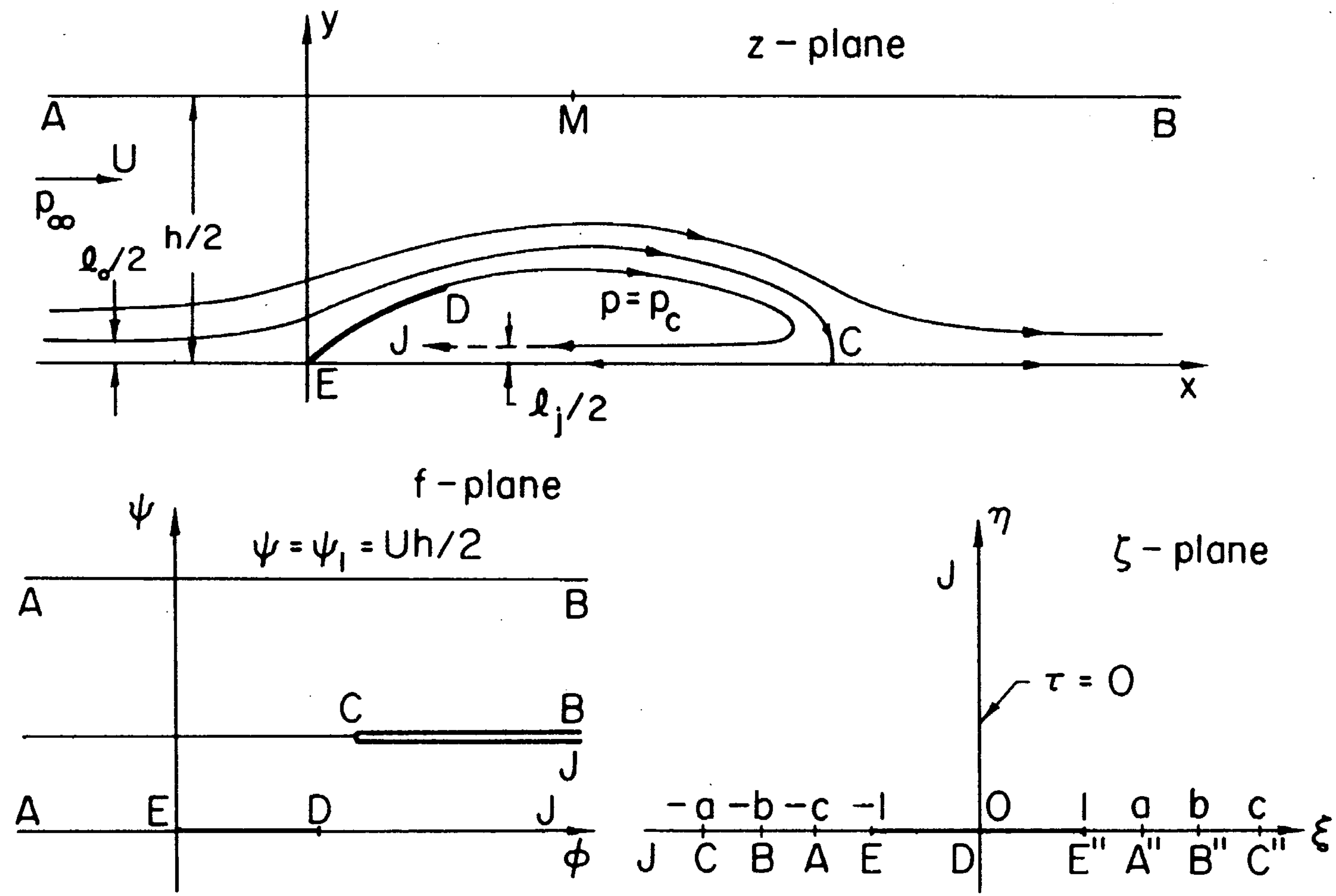

Fig. 6 The re-entrant jet model for pure drag cavity flows in a channel.

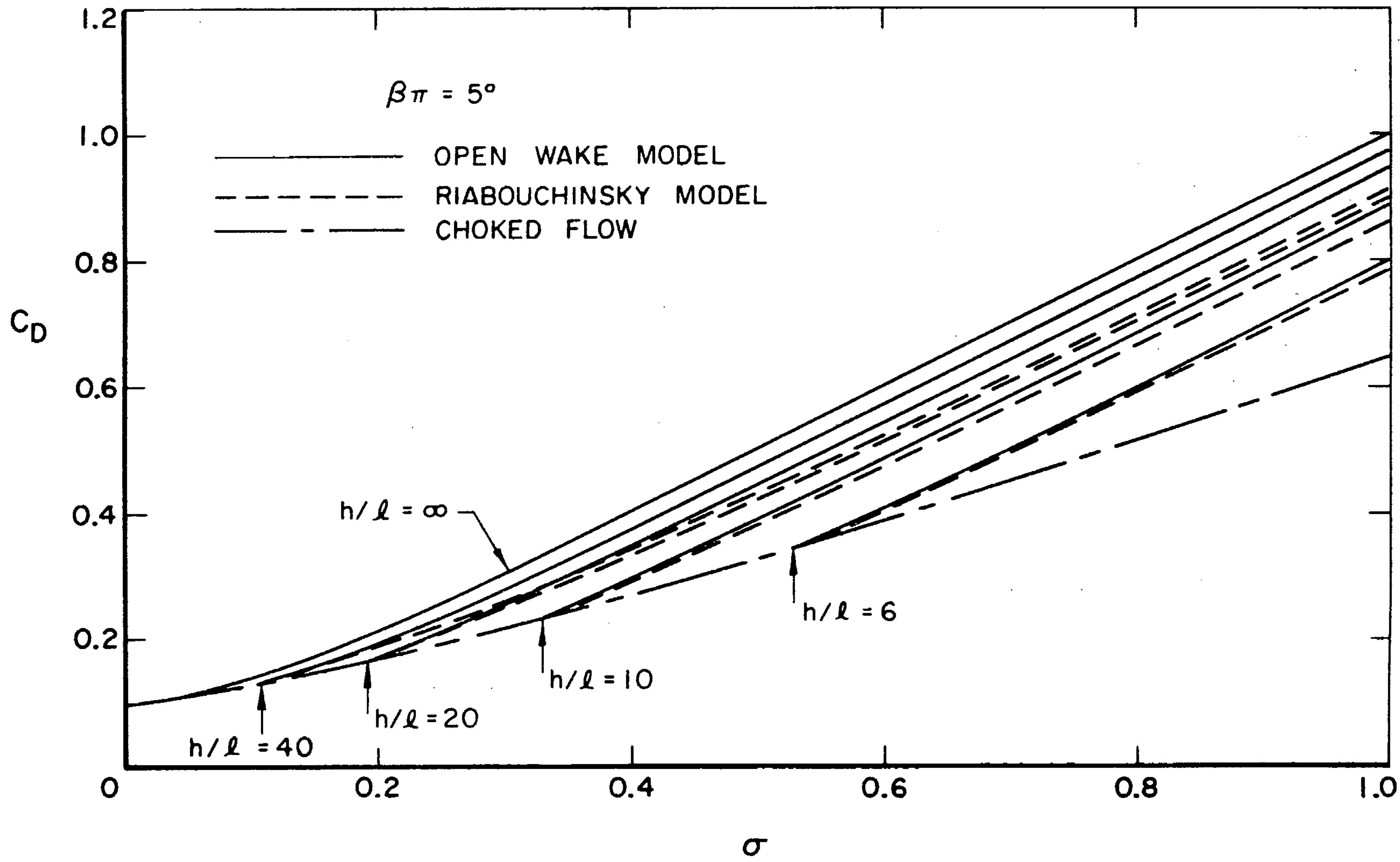

Fig. 7 Wall effect in cavity flow past a wedge, $\beta\pi = 5°$.

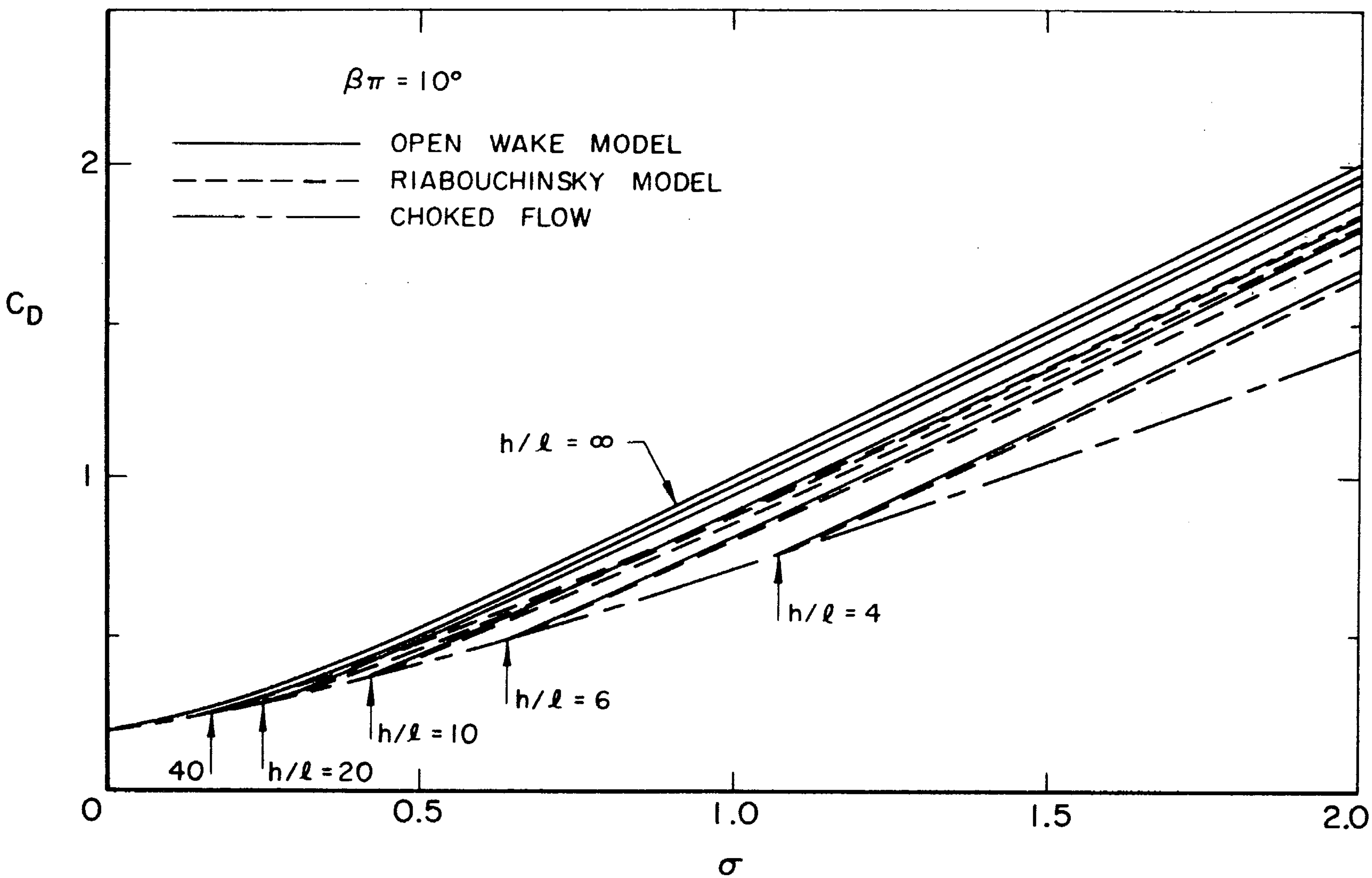

Fig. 8 Wall effect in cavity flow past a wedge, $\beta\pi = 10°$.

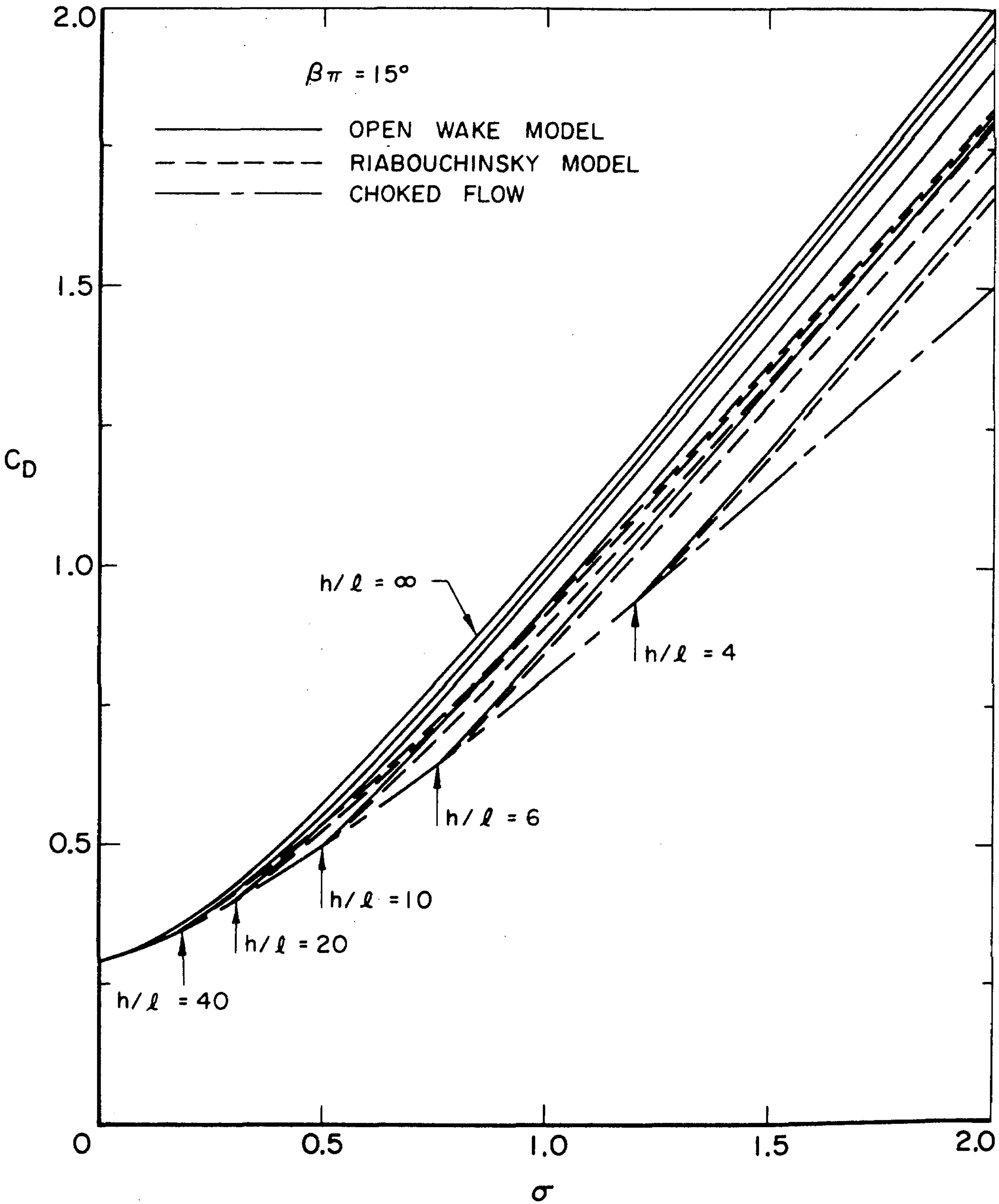

Fig. 9 Wall effect in cavity flow past a wedge, $\beta\pi = 15°$.

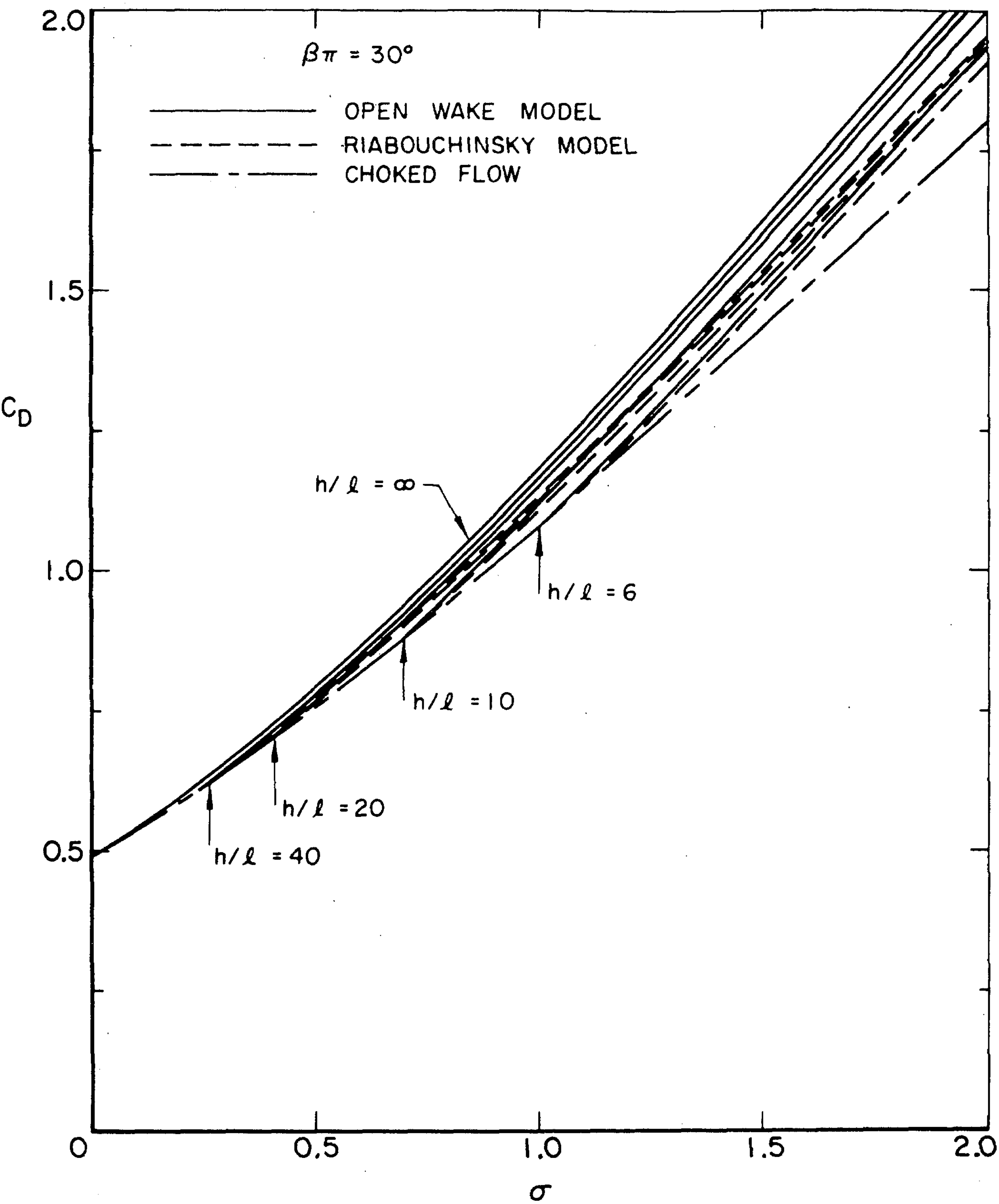

Fig. 10 Wall effect in cavity flow past a wedge, $\beta\pi = 30°$.

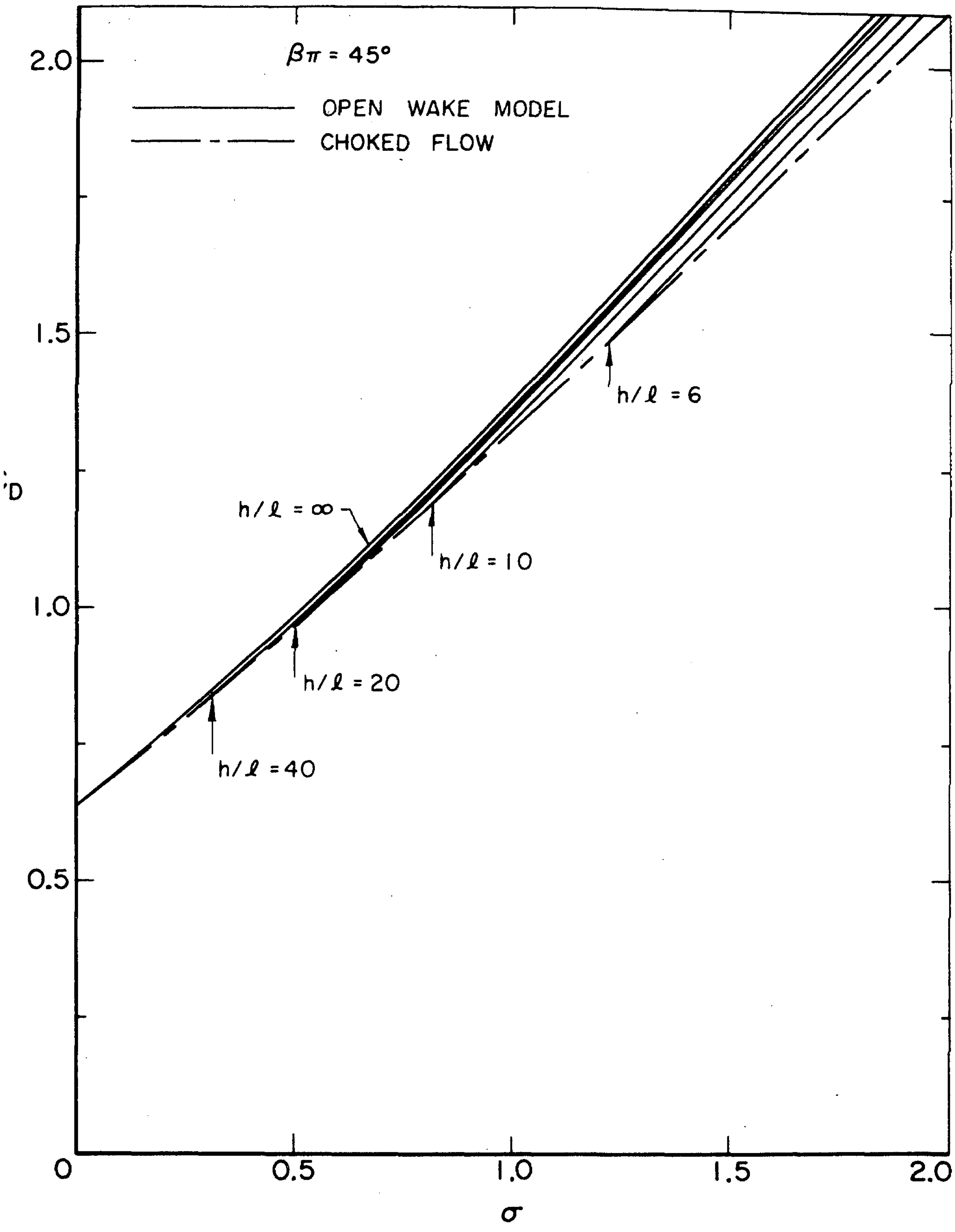

$\beta\pi = 45°$
OPEN WAKE MODEL
CHOKED FLOW
h/ℓ = ∞
h/ℓ = 6
h/ℓ = 10
h/ℓ = 20
h/ℓ = 40
2.0
1.5
1.0
0.5
0
0.5
1.0
1.5
2.0
σ

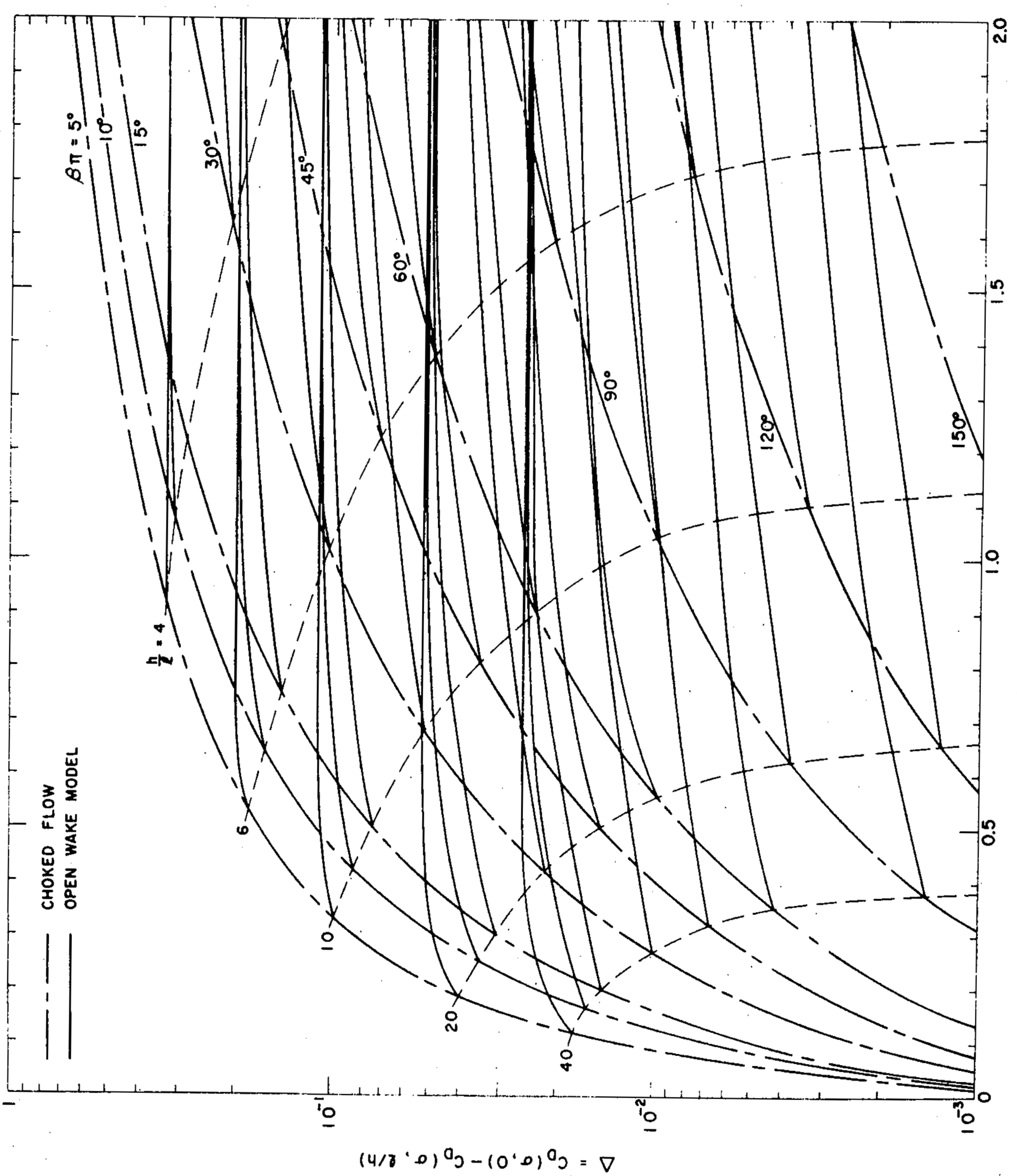

Fig. 12a Drag reduction due to the wall effect based on the open wake model.

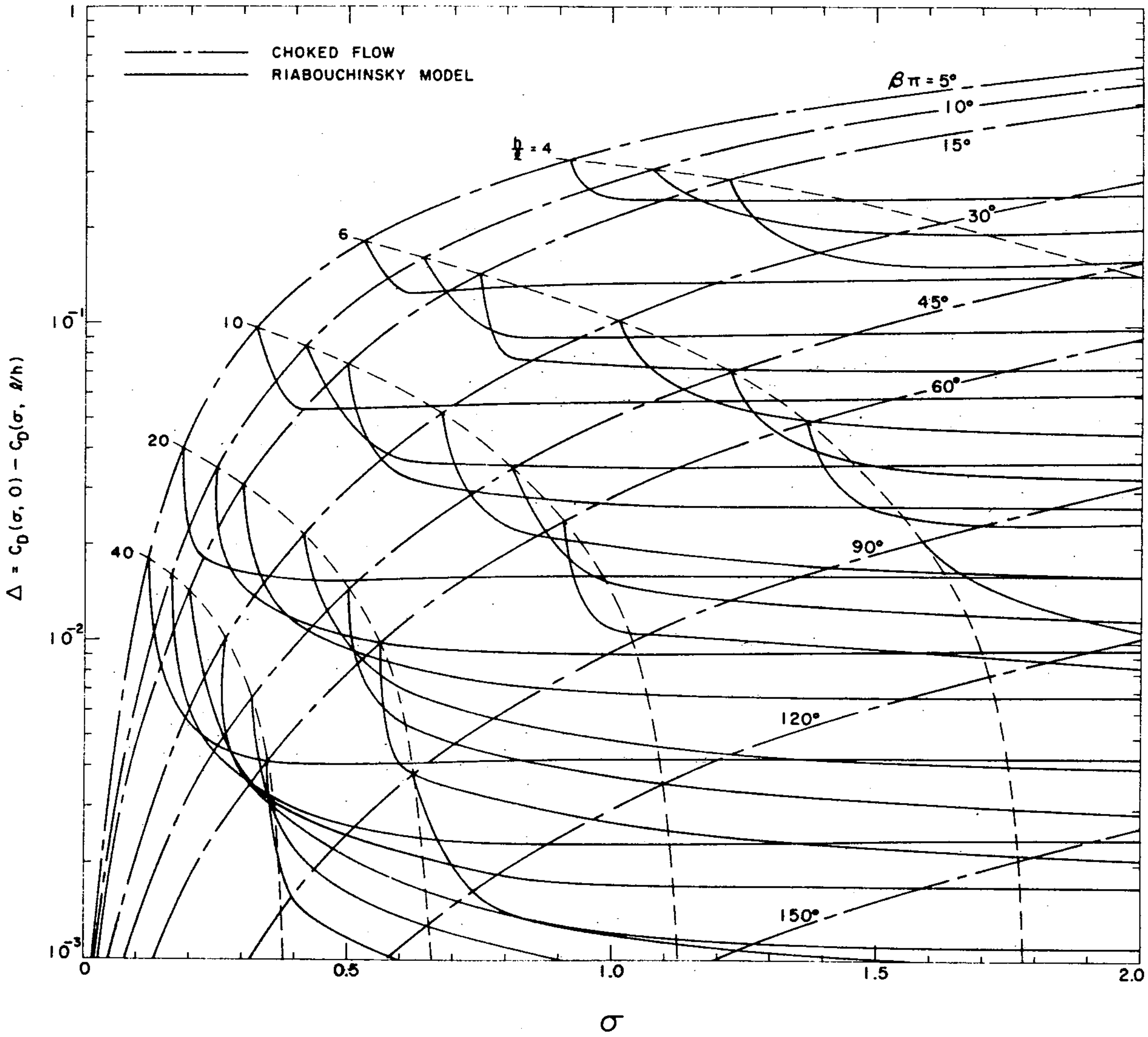

Fig. 12b Drag reduction due to the wall effect based on the Riabouchinsky model.

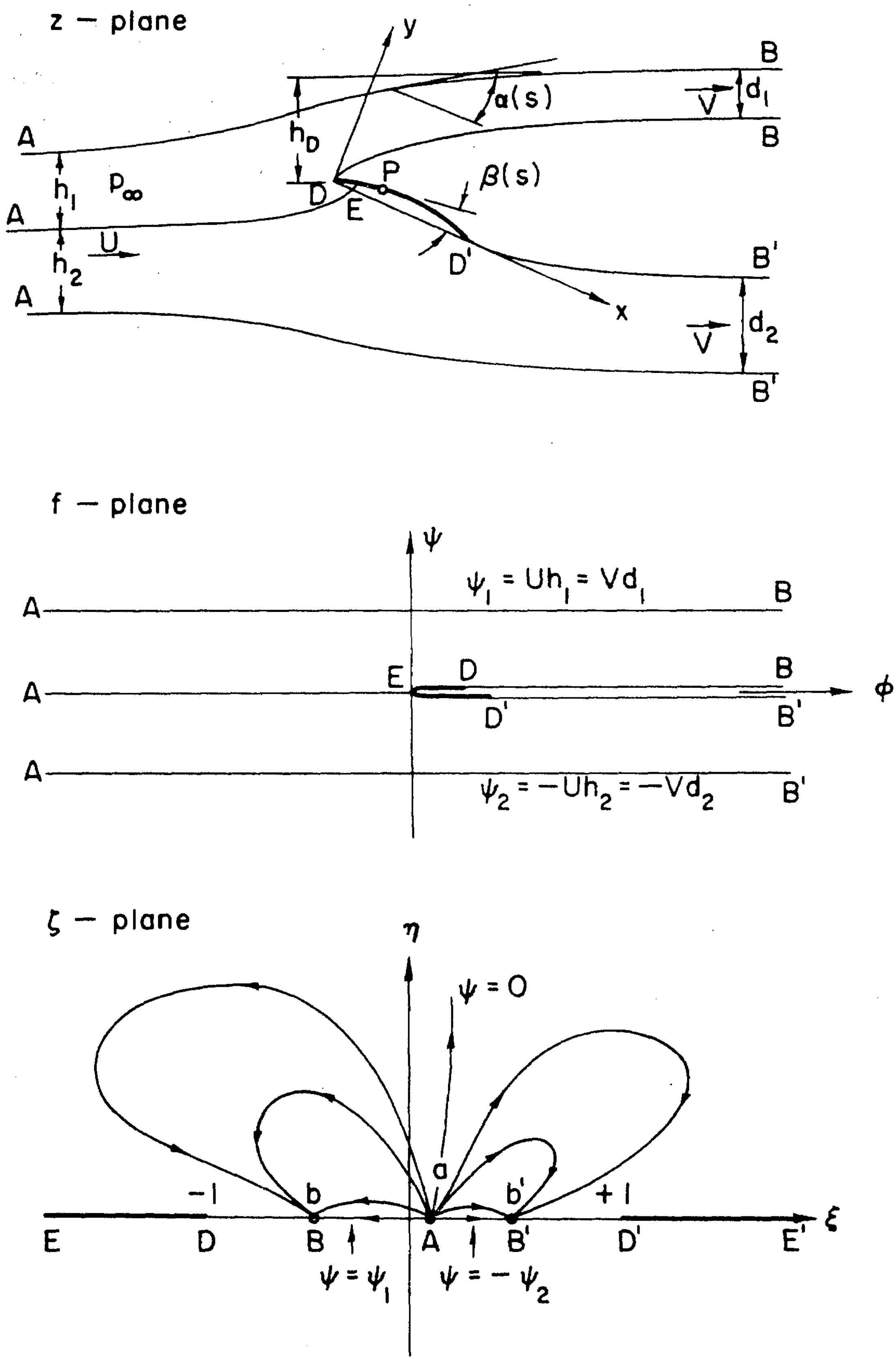

Fig. 13 Choked lifting flow past an arbitrary body in a channel.

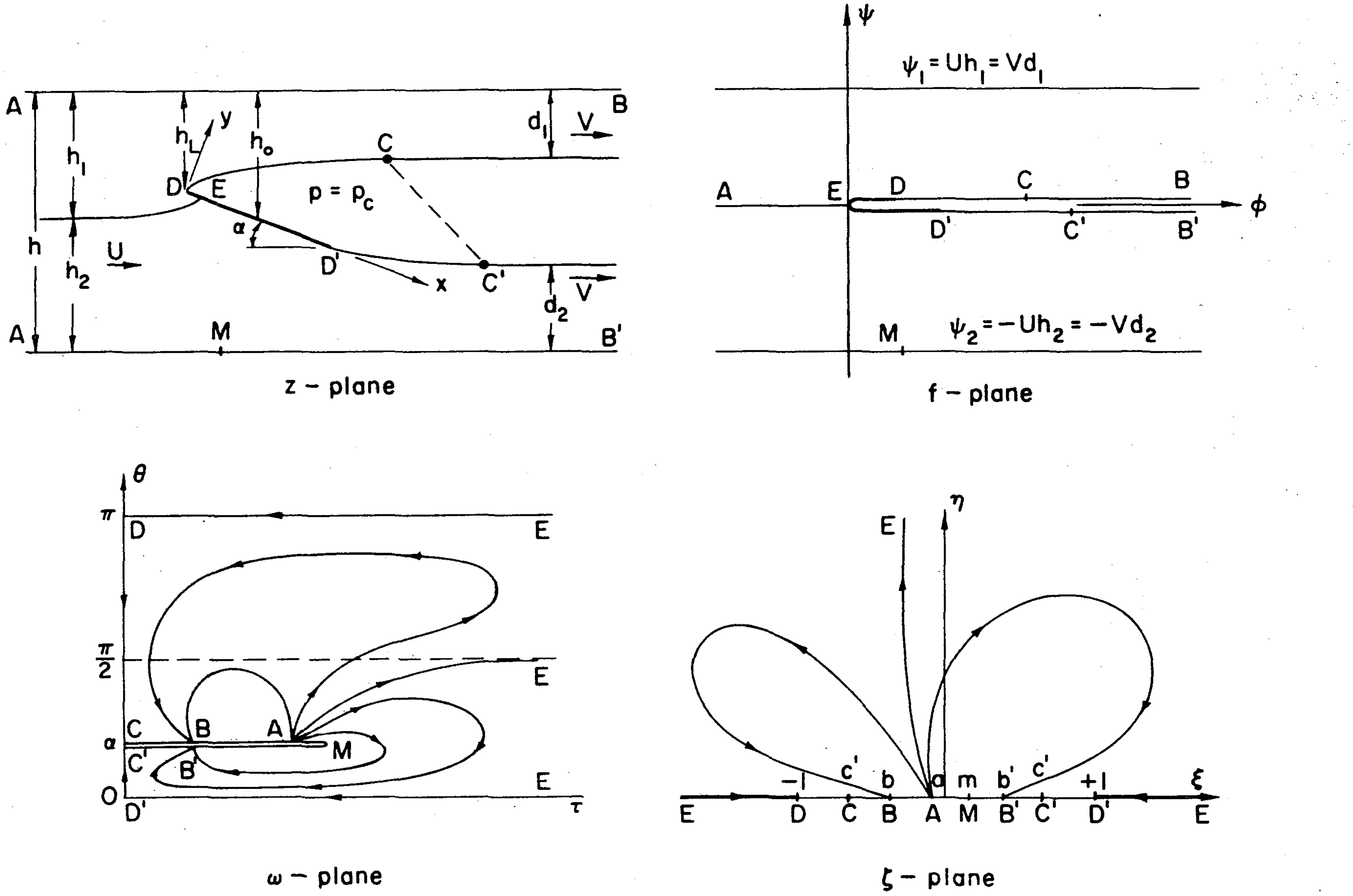

Fig. 14 The open wake model for lifting cavity flow past a flat plate in a straight channel.

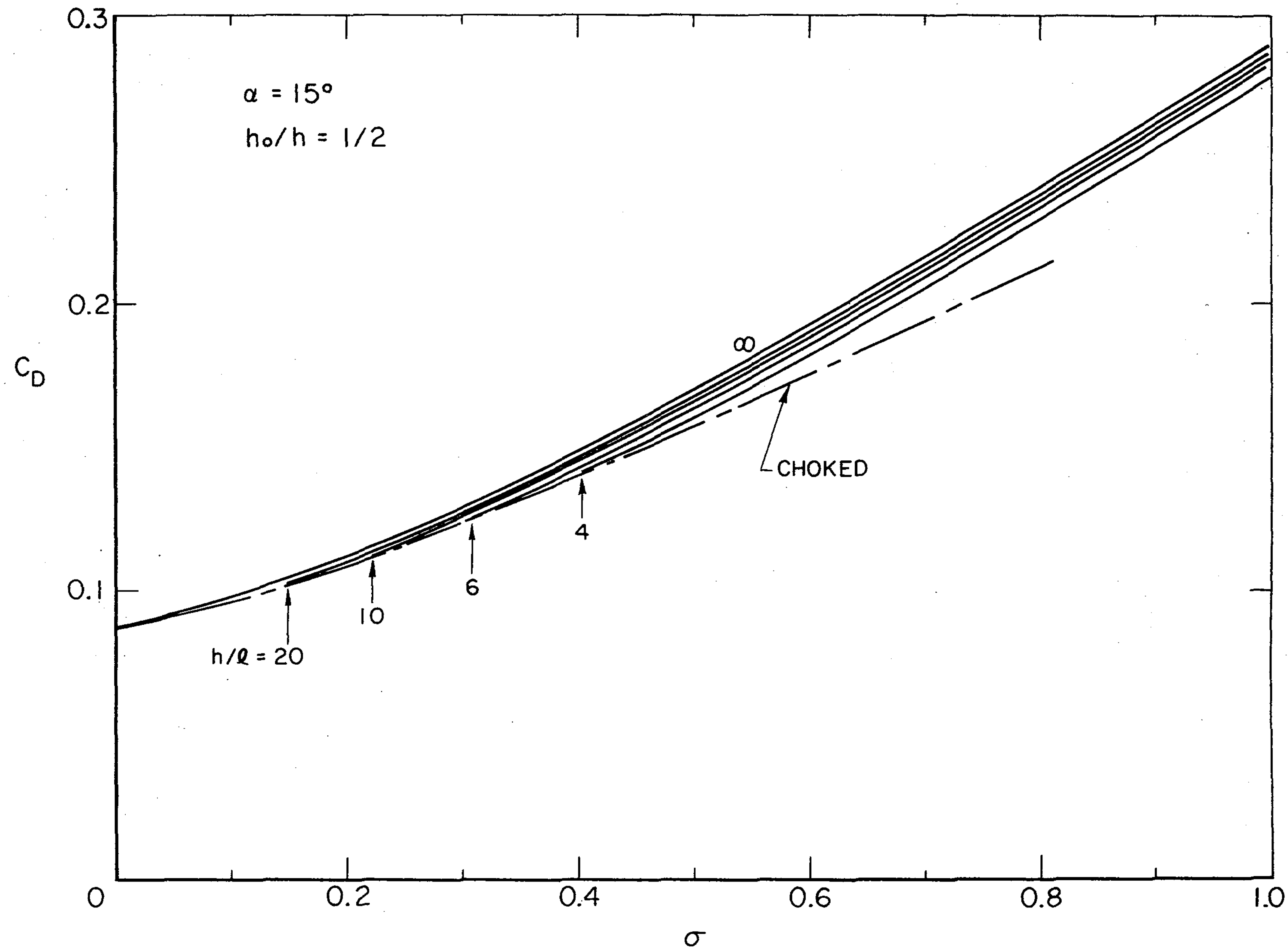

Fig. 15 Wall effect in cavity flow past an inclined flat plate, $\alpha = 15°$.

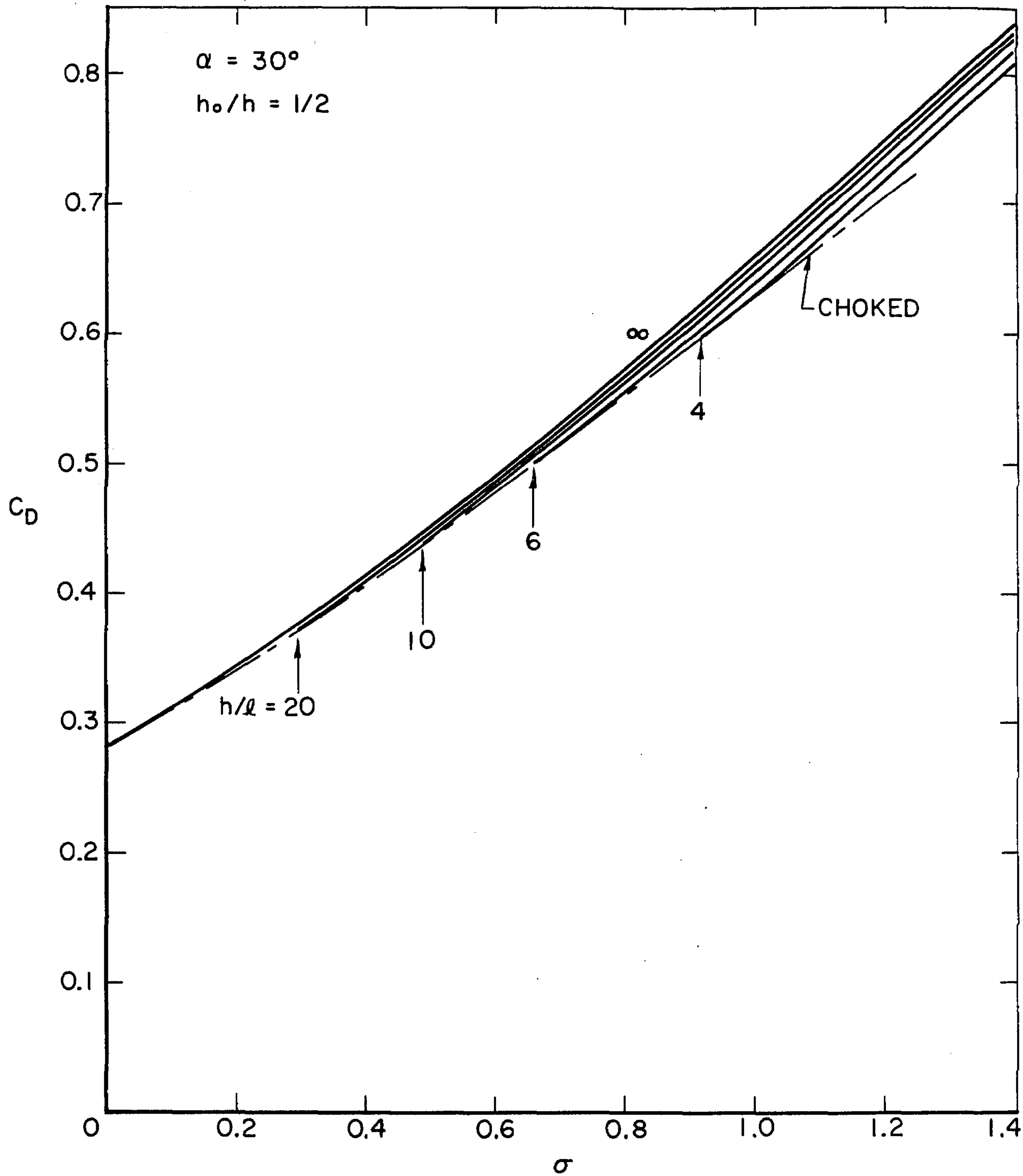

Fig. 16 Wall effect in cavity flow past an inclined flat plate, $\alpha = 30^\circ$.

Naval Ship Research and Development Center
Distribution List

Commander
Naval Ship Research and Development Ctr.
Washington, D.C. 20007
Attn: Code L41 (39)
Attn: Code 513 (1)

Commanding Officer (2)
Naval Ship Research and Development Lab.
Annapolis, Maryland 21402
Attn: Library

Commanding Officer (2)
Naval Ship Research and Development Lab.
Panama City, Florida 32402
Attn: Library

Commander
Naval Ship Systems Command
Department of the Navy
Washington, D. C. 20360
Attn: Code 0342 (1) DEF
Code 037 (1) ADF
Code 00V (1) F
Code 2052 (3)
Code PMS 81 (1) ABCDF
Code 03412 (1)

Director (20)
Defense Documentation Center
5010 Duke Street
Alexandria, Virginia 22314

Chief of Naval Research (1)
Department of the Navy
Washington, D. C. 20360
Attn: Mr. Ralph D. Cooper, Code 438

Director (1)
Office of Naval Research, Branch Office
495 Summer Street
Boston, Massachusetts 02210

Director (1)
Office of Naval Research, Branch Office
219 S. Dearborn Street
Chicago, Illinois 60604

Office of Naval Research (1)
Resident Representative
207 West 24th Street
New York, New York 10011

Chief Scientist (1)
Office of Naval Research, Branch Office
1030 East Green Street
Pasadena, California 91101

Director (1)
Office of Naval Research, Branch Office
50 Fell Street
San Francisco, California 94102

Commanding Officer (3)
Office of Naval Research, Branch Office
Box 39, Fleet Post Office
New York 09510

Commander (1)
Naval Facilities Engineering Command
Department of the Navy
Washington, D. C. 20390
Attn: Code 0321 BCDE

Commander
Naval Ship Engineering Center
Department of the Navy
Center Building, Prince Georges Center
Hyattsville, Maryland 20782
Attn: Code 6110 (1)
Code 6114D (1)
Code 6120 AC (1)
Code 6132 (1)
Code 6136 (1)
Code 6140 (1) ADEF

Strategic Systems Projects Office (1)
Department of the Navy
Washington, D. C. 20360
Attn: Dr. John Craven (NSP-001)

Commanding Officer (1)
Naval Air Development Center
Johnsville, Warminster, Pa. 18974
Attn: Technical Library

Commanding Officer and Director (11)
Naval Applied Science Laboratory
Flushing and Washington Avenues
Brooklyn, New York 11251

Officer-in-Charge
Naval Undersea Warfare Center
3202 E. Foothill Boulevard
Pasadena, California 91107
Attn: Dr. J. Hoyt (1) AD
Dr. A. Fabula (1) AD

Commander (1)
Naval Electronics Laboratory Center
San Diego, California 92152
Attn: Library DEF

Director (Code 2027) (1)
Naval Research Laboratory
Washington, D. C. 20390

Commanding Officer (1)
Navy Underwater Weapons Research
and Engineering Station
Newport, Rhode Island 02840

Commander (1)
Naval Oceanographic Office (Library)
Department of the Navy
Washington, D.C. 20390 BEF

Commander (1)
Naval Proving Ground
Dahlgren, Virginia 22448
Attn: Technical Library BDE

Commanding Officer and Director (1)
Naval Civil Engineering Laboratory
Port Hueneme, California 93401
Attn: Code L31 DE

Commander (1)
Naval Weapons Center (Code 753)
China Lake, California 93555

Commander (1)
Boston Naval Shipyard
Boston, Massachusetts 02129
Attn: Technical Library

Commander (1)
Charleston Naval Shipyard
Naval Base
Charleston, South Carolina 29408
Attn: Technical Library

Commander (1) ABCF
Long Beach Naval Shipyard
Long Beach, California 90802
Attn: Technical Library

Commander (1)
Norfolk Naval Shipyard
Portsmouth, Virginia 23709
Attn: Technical Library

Commander (1)
Pearl Harbor Naval Shipyard
Box 400, Fleet Post Office
San Francisco, California 96610
Attn: Code 246-P

Commander (1)
Philadelphia Naval Shipyard
Philadelphia, Penna. 19112
Attn: Code 240 ABCF

Commander (1)
Portsmouth Naval Shipyard
Portsmouth, N.H. 03801
Attn: Technical Library

Commander (1)
Puget Sound Naval Shipyard
Bremerton, Washington 98314
Attn: Engineering Library

Commander
San Francisco Bay Naval Shipyard
Vallejo, California 94952
Attn: Technical Library (1)
Code 250 (1)
Code 130LI (1) BDF

AFFDL (FDDS - Mr. J. Olsen) (1)
Wright-Patterson AFB
Dayton, Ohio 45433 BDE

NASA Scientific and Technical Information Facility (1)
P. O. Box 33
College Park, Maryland 20740

AFORSR (SREM) (1)
1400 Wilson Blvd. BD
Arlington, Virginia 22209

Library of Congress (1)
Science and Technology Division
Washington, D. C. 20540

U. S. Coast Guard (1)
1300 E Street N.W.
Washington, D. C. 20591
Attn: Division of Merchant Marine Safety

Director (1)
National Bureau of Standards D
Washington, D. C. 20234
Attn: Dr. G. B. Schubauer, Chief, Fluid Mechanics Branch

Director of Research, NASA (1)
600 Independence Avenue S.W.
Washington, D. C. 20546 D

Director (1)
Waterways Experiment Station
Box 631
Vicksburg, Mississippi 39180
Attn: Research Center Library BDE

Commander (1)
Naval Ordnance Systems Command
Department of the Navy
Washington, D. C. 20360
Attn: Code ORD-035 D

Commandant (E) (1)
U. S. Coast Guard (Sta 5-2)
1300 E. Street N.W.
Washington, D. C. 20591

University of Birdgeport (1)
Bridgeport, Connecticut 06602
Attn: Prof. Earl Uram, Mech. Eng. Dept. ABDE

Brown University (1)
Providence, Rhode Island 02912
Attn: Div. of Applied Math D

Naval Architecture Department
College of Engineering
University of California
Berkeley, California 94720
Attn: Library (1)
Prof. J. R. Paulling (1)
Prof. J. V. Wehausen (1)
Dr. H. A. Schade (1)

California Institute of Technology
Pasadena, California 91109
Attn: Dr. A. J. Acosta (1) ABDE
Dr. T. Y. Wu (1)
Dr. M. S. Plesset (1) BDE

University of Connecticut (1)
Box U-37
Storrs, Connecticut 06268
Attn: Prof. V. Scottron DE
Hydraulic Research Lab.

Cornell University (1)
Graduate School of Aerospace Engineering
Ithaca, New York 14850
Attn: Prof. W. R. Sears

Harvard University (1) DE
2 Divinity Avenue
Cambridge, Massachusetts 02138
Attn: Prof. G. Birkhoff, Dept. of Math.

Pierce Hall (1) D
Harvard University
Cambridge Massachusetts 02138
Attn: Prof. G. F. Carrier

University of Illinois (1)
College of Engineering
Urbana, Illinois 61801
Attn: Dr. J. M. Robertson
Theoretical and Applied Mech. Dept.

The University of Iowa (1)
Iowa City, Iowa 52240
Attn: Dr. Hunter Rouse

The University of Iowa
Iowa Institute of Hydraulic Research
Iowa City, Iowa 52240
Attn: Dr. L. Landweber (1)
Dr. J. Kennedy (1)

The John Hopkins University (1)
Mechanics Department
Baltimore, Maryland 21218
Attn: Prof. O. M. Phillips DF

Kansas State University (1) DE
Engineering Experiment Station
Seaton Hall
Manhattan, Kansas 66502
Attn: Prof. D. A. Nesmith

University of Kansas (1) D
Lawrence, Kansas 60644
Attn: Chm. Civil Engr. Dept.

Lehigh University (1)
Bethlehem, Penna. 18015
Attn: Fritz Laboratory Library

Long Island University (1)
Graduate Department of Marine Science
40 Merrick Avenue
East Meadow, N. Y. 11554
Attn: Prof. David Price

Massachusetts Institute of Technology (1)
Hydrodynamics Laboratory
Cambridge, Massachusetts 02139
Attn: Prof. A. T. Ippen DEF

Massachusetts Institute of Technology
Department of Naval Architecture and
Marine Engineering
Cambridge, Massachusetts 02139
Attn: Dr. A. H. Keil (1)
Prof. P. Mandel (1) ADE
Prof. J. R. Kerwin (1)
Prof. P. Leehey (1) DEF
Prof. M. A. Abkowitz (1) ABCDE
Prof. F. M. Lewis (1) D
Dr. J. N. Newman (1) ACD

U. S. Merchant Marine Academy (1)
Kings Point, L.I., N. Y. 11024
Attn: Capt. L. S. McCready, Head
Dept. of Engineering AB

University of Michigan
Department of Naval Architecture
and Marine Engineering
Ann Arbor, Michigan 48104
Attn: Dr. T. F. Ogilvie (1)
Prof. H. Benford (1)
Dr. F. C. Michelsen (1)

St. Anthony Falls Hydraulic Laboratory
University of Minnesota
Mississippi River at Third Avenue, S.E.
Minneapolis, Minn. 55414
Attn: Director (1)
Dr. C. S. Song (1)
Mr. J. M. Killen (1) BDEF
Mr. F. Schiebe (1) DEF
Mr. J. M. Wetzel (1) DE

U. S. Naval Academy
Annapolis, Maryland 21402
Attn: Library (1)
Dr. Bruce Johnson (1) ADF

U. S. Naval Postgraduate School
Monterey, California 93940
Attn: Library (1)
Prof. J. Miller (1) D

New York University (1)
University Heights
Bronx, New York 10453
Attn: Prof. W. J. Pierson, Jr.

New York University
Courant Institute of Mathematical
Sciences DE
251 Mercier Street
New York, New York 10012
Attn: Prof. A. S. Peters (1)
Prof. J. J. Stoker (1)

University of Notre Dame
Notre Dame, Indiana 46556
Attn: Dr. A. Strandhagen (1) BDE
Dr. J. Nicolaides (1) BD

The Pennsylvania State University
Ordnance Research Laboratory
University Park, Penn. 16801
Attn: Director (1) ABDE
Dr. G. Wislicenus (1) BDEF

Colorado State University (1)
Department of Civil Engineering
Fort Collins, Colorado 80521
Attn: Prof. M. Albertson BDEF

Princeton University (1)
Aerodynamics Laboratory
Dept. of Aerospace and Mech. Sciences
The James Forrestal Research Center
Princeton, New Jersey 08540
Attn: Prof. G. Mellor DF

Scripps Institute of Oceanography
University of California
La Jolla, California 92038
Attn: J. Pollock (1) ABCF
M. Silverman (1)

Stanford University
Stanford,California 94305
Attn: Prof. H. Ashley - Dept. of Aero and Astronautics (1)
Prof. R. L. Street (1)
Prof. B. Perry - Dept. of Civil Engineering (1)

Stevens Institute of Technology (3)
Davidson Laboratory
711 Hudson Street
Hoboken, New Jersey 07030
Attn: Dr. J. Breslin

University of Texas (1)
Defense Research Laboratory
P. O. Box 8029
Austin, Texas 78712
Attn: Director DF

University of Washington (1)
Applied Physics Laboratory
1013 N. E. 40th Street
Seattle, Washington 98105
Attn: Director ABDF

Webb Institute of Naval Architecture
Crescent Beach Road ABCD
Glen Cove, L.I., N.Y. 11542
Attn: Prof. E. V. Lewis (1)
Prof. L. W. Ward (1)

Worcester Polytechnic Institute (1)
Alden Research Laboratories
Worcester, Massachusetts 01609
Attn: Director ADE

Aerojet-General Corporation (1)
1100 W. Hollyvale Street
Azusa, California 91702
Attn: Mr. J. Levy, Bldg. 160, Dept. 4223

Bethlehem Steel Corporation (1)
Central Technical Division
Sparrows Point Yard
Sparrows Point, Maryland 21219
Attn: Mr. A. Haff, Technical Manager

Bethlehem Steel Corporation (1) ABC
Attn: H. deLuce, 25 Broadway
New York, New York 10004

Bolt Beranek and Newman, Inc. (1)
1501 Wilson Blvd.
Arlington, Virginia 22209
Attn: Dr. F. Jackson DF

Cornell Aeronautical Laboratory (1)
Applied Mechanical Department
P. O. Box 235
Buffalo, New York 14221
Attn: Dr. I. Statler BDE

Electric Boat Division (1)
General Dynamics Corporation
Groton, Connecticut 06340
Attn: Mr. V. Boatwright, Jr.

Esso International (1)
15 West 51st Street ABCD
New York, New York 10019
Attn: Mr. R. J. Taylor, Manager
R and D Tanker Department

General Applied Sciences Laboratories, Inc.
Merrick and Stewart Avenues DEF
Westbury, L.I., New York 11590
Attn: Dr. F. Lane

Gibbs and Cox, Inc. (1)
21 West Street
New York, New York 10006
Attn: Technical Library

Grumman Aircraft Engineering Corp.
Bethpage, L.I., N.Y. 11714
Attn: Mr. W. Carl

Hydronautics, Inc.
Pindell School Road
Howard County
Laurel, Maryland 20810
Attn: Mr. P. Eisenberg (1)
Mr. M. Tulin (1)

Lockheed Missiles and Space Company
P. O. Box 504 AE
Sunnyvale, California 94088
Attn: Mr. R. L. Waid, Facility No. 1
Dept. 57-01, Bldg. 150

McDonnell Douglas Aircraft Company
Douglas Aircraft Division DE
3855 Lakewood Boulevard
Long Beach, California 90801
Attn: Mr. John Hess (1)
Mr. A.M.O. Smith (1)

Measurement Analysis Corporation (1)
10960 Santa Monica Boulevard
Los Angeles, California 90025 DF

National Science Foundation (1)
Engineering Division
1800 G. Street N.W.
Washington, D.C. 20550
Attn: Director DE

Newport News Shipbuilding and
Dry Dock Company (1)
4101 Washington Avenue
Newport News, Virginia 23607
Attn: Technical Library Department

Oceanics, Incorporated (1)
Technical Industrial Park
Plainview, L.I., N. Y. 11803
Attn: Dr. Paul Kaplan

Pennsalt Chemical Corporation (1)
900 First Avenue D
King of Prussia, Penna. 19406
Attn: Mr. W. M. Lee, Director
Contract Res. Dept.

Robert Taggart, Inc. (1)
3930 Walnut Street
Fairfax, Virginia 22030
Attn: Mr. R. Taggart

Sperry-Piedmont Company (1)
Charlottesville, Virginia 22901
Attn: Mr. T. Noble

Society of Naval Architects and
Marine Engineers (1)
74 Trinity Place
New York, New York 10006

Southwest Research Institute
8500 Culebra Road BCDEF
San Antonio, Texas 78206
Attn: Dr. H. Abramson (1)
Applied Mechanics Review (1)

Sun Shipbuilding and Dry Dock Co. (1)
Chester, Pennsylvania 18013
Attn: Mr. F. Pavlik ABC
Chief Naval Architect

Tracor Incorporated (1)
6500 Tracor Lane BDF
Austin, Texas 78721

TRG/A Division of Control Data Corp. (1)
535 Broad Hollow Road (Rt. 110)
Melville, L.I., N.Y. 11746

Woods Hole Oceanographic Institute (1)
Woods Hole, Massachusetts 02543
Attn: Reference Room ABCDF

Professor Jerome Lurye (1)
Department of Mathematics
St. John's University ABCDE
Jamaica, New York 11432

Mr. B. H. Ujihara (1)
North American Aviation Inc. BD
Space and Information Systems Division
12214 Lakewood Boulevard
Downey, California 90241

Stanford Research Institute (1)
Menlo Park, California 94025
Attn: Library

Cambridge Acoustical Associates, Inc.
129 Mount Auburn Street
Cambridge, Massachusetts 02138
Attn: Dr. M. C. Junger ABDF

Dr. Roland W. Jeppson (1)
College of Engineering
Utah State University
Logan, Utah 84321

Unclassified
Security Classification

DOCUMENT CONTROL DATA - R & D

(Security classification of title, body of abstract and indexing annotation must be entered when the overall report is classified)

1. ORIGINATING ACTIVITY (Corporate author) California Institute of Technology	2a. REPORT SECURITY CLASSIFICATION Unclassified 2b. GROUP Not applicable

3. REPORT TITLE

Report No. E-111A.5

WALL EFFECTS IN CAVITY FLOWS

4. DESCRIPTIVE NOTES (Type of report and inclusive dates)

Technical Report

5. AUTHOR(S) (First name, middle initial, last name)

Wu, T. Yao-tsu
Whitney, Arthur K.
Lin, J.D.

6. REPORT DATE	7a. TOTAL NO. OF PAGES	7b. NO. OF REFS
April 1969	64	30

8a. CONTRACT OR GRANT NO. N00014-67-A-0094-0007	9a. ORIGINATOR'S REPORT NUMBER(S) Report No. E111A.5
b. PROJECT NO. SR 009 0101 and S 46-06	
c.	9b. OTHER REPORT NO(S) (Any other numbers that may be assigned this report)
d.	

10. DISTRIBUTION STATEMENT No. 1

This document has been approved for public release and sale; its distribution is unlimited.

11. SUPPLEMENTARY NOTES	12. SPONSORING MILITARY ACTIVITY Naval Ship Research and Development Center Washington, D. C., 20007

13. ABSTRACT

The wall effects in cavity flows past an arbitrary two-dimensional body is investigated for both pure-drag and lifting cases based on an inviscid nonlinear flow theory. The over-all features of various theoretical flow models for inviscid cavity flows under the wall effects are discussed from the general momentum consideration in comparison with typical viscous, incompressible wake flows in a channel. In the case of pure drag cavity flows, three theoretical models in common use, namely, the open-wake, Riabouchinsky and re-entrant jet models, are applied to evaluate the solution. Methods of numerical computation are discussed for bodies of arbitrary shape, and are carried out in detail for wedges of all angles. The final numerical results are compared between the different flow models, and the differences pointed out. Further analysis of the results has led to development of several useful formulas for correcting the wall effect. In the lifting flow case, the wall effect on the pressure and hydrodynamic forces acting on arbitrary body is formulated for the choked cavity flow in a closed water tunnel of arbitrary shape and computed for the flat plate with a finite cavity in a straight tunnel.

DD FORM 1473 1 NOV 65 (PAGE 1)

S/N 0101-807-6801

Unclassified
Security Classification

14. KEY WORDS	LINK A		LINK B		LINK C	
	ROLE	WT	ROLE	WT	ROLE	WT
Cavity flow						
Wall effect						
Wall effect correction						